



HAL
open science

Functional brain-wide network mapping during acute stress exposure in rats: Interaction between the lateral habenula and cortical, amygdalar, hypothalamic and monoaminergic regions

Laura Durieux, Karine Herbeaux, Christopher Borcuk, Cécile Hildenbrand, Virginie Andry, Yannick Goumon, Alexandra Barbelivien, Chantal Mathis, Demian Bataglia, Monique Majchrzak, et al.

► To cite this version:

Laura Durieux, Karine Herbeaux, Christopher Borcuk, Cécile Hildenbrand, Virginie Andry, et al.. Functional brain-wide network mapping during acute stress exposure in rats: Interaction between the lateral habenula and cortical, amygdalar, hypothalamic and monoaminergic regions. *European Journal of Neuroscience*, In press, 10.1111/ejn.15803 . hal-03783154

HAL Id: hal-03783154

<https://hal.science/hal-03783154v1>

Submitted on 21 Sep 2022

HAL is a multi-disciplinary open access archive for the deposit and dissemination of scientific research documents, whether they are published or not. The documents may come from teaching and research institutions in France or abroad, or from public or private research centers.

L'archive ouverte pluridisciplinaire **HAL**, est destinée au dépôt et à la diffusion de documents scientifiques de niveau recherche, publiés ou non, émanant des établissements d'enseignement et de recherche français ou étrangers, des laboratoires publics ou privés.

Functional brain-wide network mapping during acute stress exposure in rats: Interaction between the lateral habenula and cortical, amygdalar, hypothalamic and monoaminergic regions

Running title: Lateral habenula and stress network

Authors

Laura Durieux^{1*}, Karine Herbeaux¹, Christopher Borcuk¹, Cécile Hildenbrand¹, Virginie Andry^{2,3}, Yannick Goumon^{2,3}, Alexandra Barbelivien¹, Chantal Mathis¹, Demian Bataglia^{1,4,5}, Monique Majchrzak^{1*#}, Lucas Lecourtier^{1*#}

Affiliations

¹Université de Strasbourg, CNRS, Laboratoire de Neurosciences Cognitives et Adaptatives (LNCA), UMR 7364, F-67000 Strasbourg, France.

²CNRS UPR3212, Institut des Neurosciences Cellulaires et Intégratives, Centre National de la Recherche Scientifique, University of Strasbourg, Strasbourg, France.

³Mass Spectrometry Facilities of the CNRS UPR3212, Institut des Neurosciences Cellulaires et Intégratives, Centre National de la Recherche Scientifique, Strasbourg, France.

⁴University of Strasbourg Institute for Advanced Studies (USIAS), F-67000 Strasbourg, France.

⁵Université d'Aix-Marseille, Inserm, Institut de Neurosciences des Systèmes (INS) UMR-S 1106, F-1213005 Marseille, France.

*Corresponding authors: #Equal contribution

ACKNOWLEDGEMENTS

This research was supported by the CNRS, Université de Strasbourg, and a ERA-NET NEURON grant to LL (Neuromarket). The authors wish to thank Dr. Michel Barrot for the gift of CNO.

Functional brain-wide network mapping during acute stress exposure in rats: Interaction between the lateral habenula and cortical, amygdalar, hypothalamic and monoaminergic regions

ACKNOWLEDGEMENTS

This research was supported by the CNRS, Université de Strasbourg, and a ERA-NET NEURON grant to LL (Neuromarket). The authors wish to thank Dr. Michel Barrot for the gift of CNO.

Abstract

Upon stress exposure a broad network of structures comes into play in order to provide adequate responses and restore homeostasis. It has been known for decades that the main structures engaged during the stress response are the medial prefrontal cortex, the amygdala, the hippocampus, the hypothalamus, the monoaminergic systems (noradrenaline, dopamine, serotonin), and the periaqueductal gray. The lateral habenula (LHb) is an epithalamic structure directly connected to prefrontal cortical areas and to the amygdala, whereas it functionally interacts with the hippocampus. Also, it is a main modulator of monoaminergic systems. The LHb is activated upon exposure to basically all types of stressors, suggesting it is also involved in the stress response. However, it remains unknown if and how the LHb functionally interacts with the broad stress response network. In the current study we performed in rats a restraint stress procedure followed by immunohistochemical staining of the c-Fos protein throughout the brain. Using Graph Theory-based functional connectivity analyses, we confirm the principal hubs of the stress network (e.g. prefrontal cortex, amygdala, periventricular hypothalamus), and show that the LHb is engaged during stress exposure in close interaction with the medial prefrontal cortex, the lateral septum, and the medial habenula. In addition, we performed DREADD-induced LHb inactivation during the same restraint paradigm in order to explore its consequences on the stress response network. This last experiment gave contrasting results as the DREADD ligand alone, clozapine-N-oxide, was able to modify the network.

KEYWORDS

stress response, DREADD, functional connectivity, graph theory

List of Abbreviations

AAV8: Adeno-Associated Virus serotype 8	mBNST: Bed Nucleus of the <i>Stria Terminalis</i> (medial part)
ACC: Anterior Cingulate Cortex	MCC: Mid Cingulate Cortex
ACN: acetonitrile	MD: Medio-Dorsal nucleus of the thalamus
AMG: Amygdala	MHb: Medial Habenula
BA: Basal nucleus of the Amygdala	MM: Mammillary nucleus of hypothalamus
BLA: Basal Lateral nucleus of the Amygdala	MO: Medial Orbitofrontal cortex
BNST: Bed Nucleus of the <i>Stria Terminalis</i>	mPFC: medial prefrontal cortex
CamKII: CA ²⁺ /Calmodulin-dependent protein Kinase II	MR: Raphe Median
CeA: Central nucleus of the Amygdala	MS: Medial Septum
CI: Claustrum	MSpect: Mass Spectrometer
cNAc: core of the Nucleus Accumbens	PAG: Periaqueductal Gray
CNO: Clozapine-N-Oxide	PBS: Phosphate Buffered Saline
CORT: Corticosterone	PFC: Prefrontal Cortex
dCA1: dorsal <i>Cornus Ammonis</i> 1	PRh: Perirhinal cortex
dCA2: dorsal <i>Cornus Ammonis</i> 2	PRL: Prelimbic cortex
dCA3: dorsal <i>Cornus Ammonis</i> 3	PVH: Paraventricular nucleus of the Hypothalamus
dDG: dorsal Dentate Gyrus	PVT: Paraventricular nucleus of the Thalamus
dIS: dorso-lateral Striatum	Re: Reuniens nucleus
dmS: dorso-median Striatum	RS: Retrosplenial Cortex
DMSO: Dimethyl sulfoxide	sNAc: shell of the Nucleus Accumbens
DR: Raphe Dorsal	SNC: <i>Substantia Nigra pars compacta</i>
DREADD: Designer Receptor Exclusively Activated by Designer Drugs	SNr: <i>Substantia Nigra pars reticula</i>
Ect: Ectorhinal cortex	SRM: Selected Reaction Monitoring
Ent: Entorhinal cortex	SuMM: Supramammillary nucleus of the hypothalamus
hM4(Gi): modified human Muscarinic 4 (coupled with inhibitory G protein)	TS: Triangular Septal nucleus
HPA: hypothalamus-pituitary-adrenal	tVTA: tail of the Ventral Tegmental Area
HPC: Hippocampus	vCA1: ventral <i>Cornus Ammonis</i> 1
HPLC: High performance liquid chromatography	vCA2: ventral <i>Cornus Ammonis</i> 2
IL: Infralimbic cortex	vCA3: ventral <i>Cornus Ammonis</i> 3
Ins_C: Caudal part of the Insular cortex	vDG: ventral Dentate Gyrus
Ins_R: Rostral part of the Insular cortex	vis: ventro-lateral Striatum
LA: Lateral nucleus of the Amygdala	vmS: ventro-median Striatum
IBNST: Bed Nucleus of the <i>Stria Terminalis</i> (lateral part)	VO: Ventral Orbitofrontal cortex
LC: Locus Coeruleus	VP: Ventral Pallidum
LDT: Latero-dorsal Tegmental nucleus	VTA: Ventral Tegmental Area
LH: Lateral Hypothalamus	
LHb: Lateral Habenula	
LHbL: Lateral part of the Lateral Habenula	
LHbM: Medial part of the Lateral Habenula	
LO: Lateral Orbitofrontal cortex	
LS: Lateral Septum	

1 INTRODUCTION

2 Adaptive response to stress exposure requires the coordinated activity of an extended brain network
3 involved in cognitive, emotional, and motor processes (Joëls and Baram, 2009; Godoy et al., 2018).
4 A large part of the studies addressing stress-induced changes in such functional network did so in
5 the context of chronic stress, in order to better understand pathological conditions (e.g. Henckens et
6 al., 2015; Magalhães et al., 2018). In humans, acute stressors engage key regions such as the insula
7 (Ins), amygdala (AMG), anterior cingulate cortex (ACC), ventral striatum, prefrontal cortex (PFC),
8 hippocampus (HPC), bed nucleus of the stria terminalis (BNST), thalamus, and the paraventricular
9 nucleus of the hypothalamus (PVH) (Herman et al., 2003; Sousa, 2016). These structures – or their
10 homologous regions - have also been shown to subservise physiological and behavioral responses to
11 stress exposure in rodents (Herman et al., 2003; McEwen et al., 2015; Godoy et al., 2018).

12 In recent years, the lateral habenula (LHb), an epithalamic structure integrating forebrain information
13 and modulating the activity of the main monoaminergic pathways, emerged as a prominent region
14 for the control of the stress response (Hikosaka, 2010; Hu et al., 2020). The LHb is strongly activated
15 by acute exposure to various stressors ranging from mild ones, like exposure to a novel environment
16 (Wirtshafter et al., 1994; Durieux et al., 2020), to more severe such as electrical foot-shock,
17 immobilization, tail pinch, and predator exposure (Chastrette et al., 1991; Wirtshafter et al., 1994;
18 González-Pardo et al., 2012; Brown and Shepard, 2013; Dolzani et al., 2016; Zhang et al., 2016;
19 Lecca et al., 2017; Barrett and Gonzalez-Lima, 2018; Durieux et al., 2020). Interestingly, in rodents
20 the LHb directly or indirectly interacts with the above-cited key regions of the stress response.
21 Regions which send direct projections onto the LHb comprise the entire PFC (Kim and Lee, 2012),
22 and the extended amygdala, including the BNST (Dong and Swanson, 2004, 2006) and central
23 amygdalar nucleus (Zhou et al., 2019). The LHb and HPC, although they do not share direct
24 connections, likely communicate and functionally interact (Aizawa et al., 2013; Goutagny et al., 2013;
25 Baker et al., 2019). The LHb has been shown to modulate the hypothalamus-pituitary-adrenal (HPA)
26 axis (one of the primary effectors of the stress response; Selye, 1950; de Kloet et al., 1998), and
27 therefore most likely the activity of the PVH (Murphy et al., 1996; Jacinto et al., 2016; Mathis et al.,
28 2018). In addition, the LHb, as shown in rodents, cats and monkeys, can modulate the main
29 neurotransmitter systems involved in the stress response, *i.e.*, dopamine (Christoph et al., 1986; Ji
30 and Shepard, 2007; Lecourtier et al., 2008), noradrenaline (Kalen, 1989a; Cenci et al., 1992), and
31 serotonin (Reisine et al., 1982; Kalen et al., 1989b). The link with the serotonergic system is of
32 particular interest as inhibition of the LHb-dorsal raphe nucleus pathway in rats reduces passive
33 stress response (Coffey et al., 2020). The LHb also interacts with other regions to process emotional
34 responses. For example, in mice inhibition of the lateral hypothalamus-LHb pathway alters escape
35 behavior upon unpredictable exposure to foot-shocks (Lecca et al., 2017), and stimulation of the
36 pathway connecting the entopeduncular nucleus to the LHb (Shabel et al., 2012), the LHb to the
37 ventral tegmental area (Lammel et al., 2012), and the LHb to the rostromedial tegmental nucleus

38 (Stamatakis and Stuber, 2012), induces aversive responses. Finally, probably through an indirect
39 activation of rostral medullary raphe neurons, the LHb has been involved in rats in the control of
40 stress-induced hyperthermia, a component of the physiological stress response (Ootsuka et al.,
41 2017).

42 To date no study has been devoted to unravelling if and how the LHb is part of the broad network
43 involved in the stress response. In the current study we used acute exposure to restraint stress as a
44 behavioural paradigm and specifically aimed to describe: 1) the network activated by restraint and
45 the position of the LHb within this network, and 2) the consequences of DREADD-induced LHb
46 inactivation on the connectivity of the network. To this aim we quantified the level of expression of
47 the c-Fos protein in a large number of brain regions, including the key structures involved in the
48 acute stress response. The immediate-early gene c-Fos appeared relevant to explore as it is the
49 best characterized and most widely used tool for functional anatomical mapping in rodents, given its
50 rapid activation by various stimuli (Kovács, 1998; Hudson, 2018). The quantification of the density
51 of c-Fos positive (c-Fos+) cells throughout the brain, and the exploration of between-structure
52 correlations can reveal functional interactions between structures belonging to a given network, as
53 several studies previously argued (e.g., in fear memory; Wheeler et al., 2013; Vetere et al., 2017).
54 This level of analysis can be achieved applying a Graph theory approach. Graph theory is a
55 mathematical field allowing to analyze complex networks (Bullmore and Sporns, 2009). The main
56 principle of this approach is to consider the structures as nodes of a given network, nodes that are
57 connected through edges (the functional variable, in our study, c-Fos+ cells density correlations).
58 Then, different parameters of the network can be revealed, such as the principal hubs of the network,
59 though strength analysis, or the presence of sub-networks, which could be engaged in different
60 aspects of the ongoing process, through the extraction of modules/communities (see Bullmore and
61 Sporns 2009 for examples). Finally, in animals exposed to restraint, we assessed the level of
62 plasmatic corticosterone, before and following restraint, in order to control for the effectiveness of
63 such procedure and to further investigate if the LHb modulates the HPA axis upon stress exposure.

64

65 MATERIALS & METHODS

66 **Animals**

67 This experiment, authorized by the French authorities (APAFIS#7114), was carried out with 44 five
68 months old male Long–Evans rats (Janvier Labs, France) issued from a previous study (Durieux et
69 al., 2020). They were housed in pairs on a 12 h light/dark cycle (lights on at 7:00 A.M.) with *ad libitum*
70 access to food and water. Rats were singly housed five days before the start of the experiment and,
71 the last three days, were familiarized to the holding procedure later used to collect blood samples.
72 The experiment took place between 9:00 and 12:00 PM. A schematic representation of the
73 experimental procedure is provided in **Figure 1**.

74 **Surgery**

75 Surgery was conducted 7-9 weeks before the experiment as described in detail in Durieux et al.
76 (2020). Shortly, under isoflurane anesthesia [4% for induction; 1.5 % throughout surgery] and
77 painkiller supply (meloxicam, 1 mg/kg, s.c.), rats were bilaterally microinjected with either the viral
78 vector (AAV8–CamKII–hM4(Gi)–mCherry; Viral Production Unit, Universitat Autònoma de
79 Barcelona; hM4 animals, n=22), or phosphate–buffered saline (PBS animals; n=22) at the two
80 following coordinates and volumes : 1) anteroposterior (AP) = – 3.3 mm from Bregma, mediolateral
81 (ML) = ± 0.7 mm from the midline of the sagittal sinus, dorsoventral (DV) = – 4.5 mm from dura (0.2
82 µL); 2) AP = – 3.5 mm from Bregma, ML = ± 0.7 mm from the midline of the sagittal sinus, DV = –
83 4.4 mm from dura (0.15 µL).

84 **Drug treatments**

85 Rats were allocated to CNO (1 mg/kg; dissolved in 0.9% NaCl–0.5% DMSO; *i.p.*) or vehicle (Veh,
86 0.9% NaCl–0.5% DMSO, *i.p.*) treatment as in our previous study (Durieux et al., 2020; see
87 Supporting information **Table S1**). Thirty minutes after drug injection, animals of each treatment
88 condition were either exposed to blood sampling and restraint [restraint stress (RS) groups], or
89 remained undisturbed in their home cage [home cage (HC) group]. More precisely, sixteen hM4
90 animals and sixteen PBS animals were administered CNO and pseudo-randomly distributed in the
91 two behavioural conditions as follows: home-cage condition [HC; hM4–CNO–HC group (n=8) and
92 PBS–CNO–HC group (n=8), respectively] or restraint stress condition [RS; hM4–CNO–RS group
93 (n=9) and PBS–CNO–RS group (n=7), respectively]. Six rats injected with PBS and six rats injected
94 with AAV8–CamKII–hM4(Gi)–mCherry (to control for the potential effects of the expression of both
95 the hM4 receptors and the mCherry fluorophore) were administered vehicle (Veh); those rats
96 composed the two Veh control groups, such as it was done in Durieux et al. (2020), each composed
97 of 3 rats injected with PBS and 3 rats injected with AAV8–CamKII–hM4(Gi)–mCherry, and named
98 (PBS or hM4)–Veh–HC and (PBS or hM4)–Veh–RS according to the behavioral condition they were
99 pseudo-randomly assigned to, home cage and restraint stress respectively.

100

101 **Restraint**

102 Rats were gently placed in an opaque grey PVC tube (length, 80 cm; diameter, 13.5 cm) including
103 ventilation holes at each end. They remained in it for a duration of 10 min.

104 **Plasmatic CORT concentration assessment**

105 *Blood sampling*

106 Blood sampling was performed in RS groups 2 min before (pre-restraint) and 2 min after (post-
107 restraint) the restraint procedure. Rats were put on a table with their head positioned in a folded
108 towel, and gently held in place. The caudal vein was lightly incised with a razor blade and blood,
109 approximately 250 µl each time, was collected through a heparinized capillary tube (Microvette CB
110 300) while gently stroking the tail from the base to the tip. The pre-restraint incision was performed
111 about 3 cm from the tip of the tail, and the post-restraint one was performed 2 cm higher. As soon
112 as blood was collected, the tubes were placed in ice (4°C) before being centrifuged (3000 rpm at
113 4°C during 4 min) to collect approximately 150 µl of plasma, which was then stored at -80°C until
114 analysis was performed.

115 *CORT preparation*

116 For each sample, 50 µl of plasma were added to 10 µl of D4-CORT (50 pmole/10 µl, Sigma-Aldrich,
117 St. Quentin Fallavie, France) in 99.1% H₂O / 0.1 % formic acid (v/v). Then, proteins were precipitated
118 by adding 1 ml of acetonitrile (ACN 100 %). Two successive centrifugations were performed at
119 20,000 g (4°C, 20 min) and, the resulting supernatant was recovered and dried under vacuum
120 (SpeedVac, Thermo Fisher). Samples were re-suspended in 30 µl of 20 % ACN / 0.1 % of formic
121 acid, followed by a last centrifugation (20,000 g, 10 min). Supernatants were recovered and kept at
122 -80°C until LC-MS/MS analysis.

123 *Liquid Chromatography Tandem-mass Spectrometry (LC-MS/MS)*

124 Analyses were performed with a Dionex Ultimate 3000 HPLC system (Thermo Electron, Villebon-
125 sur-Yvette, France) coupled with a triple quadrupole Endura mass spectrometer (Thermo Electron).
126 Samples were loaded onto a ZORBAX SB-C18 column (150 x 1 mm, 3.5 µm, flow of 90 µl/min;
127 Agilent, Les Ulis, France) heated at 40°C. LC and MS conditions used are detailed in Supporting
128 information **Table S2-3**. Qualification and quantification were performed using the multiple reaction
129 monitoring mode (MRM) according to the isotopic dilution method (Ho et al., 1990). Identifications of
130 the compounds were based on precursor ions, selective fragment ions and retention times obtained
131 for the heavy counterpart (*i.e.*, IS). Selection of the monitored transitions and optimisation of collision
132 energy and RF Lens parameters were determined automatically (Supporting information **Table S3**).
133 Xcalibur v4.0 software was used to control the system (Thermo Electron).

134 **Brain tissue preparation and section processing**

135 Eighty minutes after the end of the restraint stress procedure, rats were deeply anesthetized with a
136 pentobarbital overdose (120 mg/kg, *i.p.*). Following intracardiac perfusion of phosphate-buffered
137 saline (PBS, 0.1M) and then 4% paraformaldehyde (PFA)-PBS solution (pH 7.4; 4°C), brains were

138 removed, post-fixed in 4 % PFA-PBS (4°C, 2 h), transferred into a 0.1 M PBS–20 % sucrose solution
139 (4°C, 48 h) and subsequently frozen (isopentane, - 40°C, 1 min). Serial 40 µm-thick free-floating
140 sections were cut – 1 every 120 µm – in the coronal plane at – 20°C and stored in a cryoprotectant
141 solution at – 20°C (see Supporting information **Table S4** for a detailed description of the coordinates
142 of the boundaries of the different structures investigated according to the Paxinos and Watson
143 stereotaxic atlas). In animals injected with the DREADD viral solution, within the block containing the
144 LHb, one every three sections were directly collected on gelatin-coated slides in order to assess the
145 extent of mCherry expression.

146 ***c-fos Immunohistochemistry***

147 The immunohistochemistry protocol used was performed such as during our previous study (see
148 Durieux et al., 2020 for details). In summary, c-Fos proteins were bound by primary anti-Fos rabbit
149 polyclonal antibody (1:750, polyclonal rabbit antibodies; SYSY; ref: 226 003, Synaptic System). The
150 secondary antibody was a biotinylated goat anti-rabbit antibody (1:500, Biotin-SP-conjugated
151 affiniPure Goat anti-rabbit IgG, ref: BA1000, Vector). Staining was performed with the avidin–biotin
152 peroxidase method (Vectastain ABC kit, PK 6100; Vector Laboratories, Burlingame, CA, USA).
153 Sections were subsequently mounted on gelatin-coated slides, dehydrated by incrementally
154 concentrated alcohol baths (70%, 90%, 95%, 100%, 100%), covered with Clearify (Americain
155 MasterTech Scientific) and covered with Diamount (Diapath S.P.A). In addition, in rats in which LHb
156 contained hM4(Gi) receptors and which were administer CNO during HC and RS conditions, we
157 performed fluorescent c-fos immunohistochemistry staining on slices containing the LHb. Slices
158 (from 3 to 6 per rat) adjacent to the ones used for the previously performed DAB/bright field c-Fos
159 immunohistochemistry were chosen. Floating slices were exposed to a primary anti-Fos guinea pig
160 antibody (1:1000, ref: 226005, Synaptic Systems) followed by exposure to a goat anti-guinea pig
161 secondary antibody (1:500, ref A-11073, ThermoFisher) coupled to Alexa Fluor 488. Slices were
162 then mounted on gelatin-coated slides and covered with a DAPI–fluoromount medium. Sections
163 were scanned and saved in NDPI format using a NanoZoomer S60 (Hamamatsu) at x 20 thanks to
164 the associated software (NDP.scan, Hamamatsu) [c-Fos, 488 nm (FITC filter); mCherry, 594 nm
165 (TRITC filter)].

166 ***Quantification***

167 Quantification of c-Fos positive (c-Fos+) cells revealed with avidin-biotin method was performed in
168 56 structures (see Supporting information **Figure S1-2**) using a semi-automated method with
169 ImageJ (Free License, Wayne Rasband, Research Services Branch, National Institute of Mental
170 Health, Bethesda, Maryland, USA; testing of the accuracy of the method is presented in Supporting
171 information **Figure S3**) such as described in Durieux et al. (2020). We took from 3 to 20 sections per
172 structure depending on their rostro-caudal extent. Both hemispheres were pooled. Results were
173 expressed as mean number of c-Fos+ cells by mm² (for more details see Supplementary
174 information). Quantification of LHb cells that were c-Fos positive (c-Fos+) and mCherry positive

175 (mCherry+) was performed using the software QuPath (Bankhead et al., 2017). First, the LHb was
176 manually outlined on each slices (3 to 6 per rat) using outlines identical to those used for the
177 previously performed DAB/bright field c-Fos immunohistochemistry. Then we extracted the number
178 of fluorescent cells in the two filters based on the detection cells algorithm; the settings used were
179 as follows: background radius (8 μm), sigma (1.5 μm); the cell area was expected to be between 10
180 and 400 μm so that the threshold was set to 10. Once the detection of the cells terminated the area
181 of the overlay was saved along with the number of detected cells in each wavelength. The density
182 of both c-Fos+ and mCherry+ cells (in number/ mm^2) was calculated dividing the number of the cells
183 detected by the area delimited by the overlay. The number of cells that were both c-Fos+ and
184 mCherry+ (colocalization; c-Fos+/mCherry+) was counted manually in the same defined areas.

185 **Statistical analyses**

186 Between-group [(PBS or hM4)-Veh, PBS-CNO, and hM4-CNO in the RS condition] comparison of
187 plasmatic corticosterone (CORT) levels was performed using a two-way ANOVA with Time (pre- vs
188 post-restraint) as the repeated measure. For each brain region, c-Fos raw data (c-Fos+ cells
189 densities) were analyzed with ANOVAs with Group [(PBS or hM4)-Veh, PBS-CNO, hM4-CNO] and
190 Condition (HC and RS) as between-subject factors. Post hoc Newman-Keuls multiple range test was
191 used when appropriate. In all analyses significance was set for $p < 0.05$.

192 **Functional connectivity analysis**

193 We used this analysis method to model the functional network during stress response. For this
194 purpose, only c-Fos data of the RS groups were further analyzed using network modeling [(PBS or
195 hM4)-Veh-RS, $n=6$; PBS-CNO-RS, $n=7$; hM4-CNO-RS, $n=7$]. They were processed using Python
196 (version 3.7.5, PyCharm edition community – free; <https://www.jetbrains.com/fr-fr/pycharm/>) with
197 helps from several toolbox. For general coding, we used pandas (manipulating data as DataFrame
198 and XLSX/CSV export/import; <https://pandas.pydata.org/>), numpy (managing matrix;
199 <https://numpy.org/>), Scipy (for general statistic purposes; <https://www.scipy.org/>). The others Python
200 toolbox used during the analysis for precise goal are cited when necessary. Correlations were
201 calculated using Korr (<https://pypi.org/project/korr/>) according to the Pearson method. The
202 correlation matrix was plot using matplotlib (<https://matplotlib.org/>) and seaborn
203 (<https://seaborn.pydata.org/>). The 3D Rats brains representations used have been created from The
204 Scalable Brain Atlas (Bakker et al., 2015).

205 The network modeling was processed using NetworkX toolbox (<https://networkx.org/>). The graphs
206 were undirected and unsigned (absolute correlations were used as weights). All analyses were done
207 on full weighted networks. Graph theoretical metrics, *i.e.*, the strength of each node in the network,
208 the modularity (based on Louvain algorithm module/community detection, see below), the average
209 clustering coefficient, and the average of edge weights, were computed using NetworkX. We used
210 classical bootstrap analysis to estimate the variance of the population in groups or in random model.
211 The random model was computed by shuffling the row and the column of the correlation matrix

212 keeping the main diagonal intact (so that each structure remains the same in the random model).
213 Between-group comparisons were done using the permutation test. The permutation test is a
214 statistical test under the null hypothesis based on the calculation of the shuffling of the two compared
215 groups (creating the null hypothesis) and comparing the given distribution of the p value to the p
216 value of both original groups. Only data showing a significance difference ($p < 0.05$) in both tests
217 (bootstrap and permutation) were estimate significantly different.

218 The allegiance matrices were computed using the Louvain method which allows to unfold
219 communities in large networks (Python package <https://pypi.org/project/python-louvain/> called by
220 NetworkX). The modules (or communities) were calculated for each bootstrap, modulating the
221 resolution of Louvain algorithm from 0.88 to 1 over 10 repetitions, so that the number of communities
222 varied from 2 to 5 depending on the group considered (see Supporting information **Figure S4**). The
223 allegiance represents the probability that two structures are in the same community across bootstrap
224 iterations over all possible pair of structures. The allegiance matrix also displays modules, allowing
225 us to extract the communities on this matrix and study which structures may be activated in a
226 functionally coordinated manner. This calculation can highlight high synchronicity and high functional
227 connectivity between structures of the same community. Once the allegiance matrix calculated, the
228 allegiance communities were extracted using the Louvain algorithm (resolution of 1). The allegiance
229 communities of the (PBS or hM4)-Veh-RS group was extracted and the “within-module strength Z-
230 score” evaluated (see Supporting information **Figure S4**).

231 Between-group comparisons were based on the communities extracted from the (PBS or hM4)-Veh-
232 RS group. The average strength of the structures of each community was calculated for each group
233 and compared (PBS or hM4)-Veh-RS vs PBS-CNO-RS, (PBS or hM4)-Veh-RS vs hM4-CNO-RS
234 and PBS-CNO-RS vs hM4-CNO-RS) using the non-parametric test, Wilcoxon-Mann-Whitney. The
235 differences were considered significant for $p < 0.05$. On the same principle, we also tested the
236 possible differences between the PBS-CNO and the hM4-CNO communities based on PBS-CNO
237 communities. For each group we assessed the distribution of the structures of interest in the different
238 communities, using the so-called confusion matrices, based on the principle that communities do not
239 have a hierarchical level, so that one may wonder which community of a given group best represents
240 the community of another group. We calculated the Jaccard index gauging the similarity and the
241 diversity of a sample set.

242

243 RESULTS

244 *Histology*

245 Following histological verification (extend of mCherry staining), groups were composed as follows:
246 (PBS or hM4)-Veh-HC, n = 6; (PBS or hM4)-Veh-RS, n = 6; PBS-CNO -HC, n = 8; PBS-CNO -RS,
247 n = 7; hM4-CNO-HC, n = 4; hM4-CNO-RS, n = 7. The extent of the expression of mCherry in hM4-
248 CNO animals is represented in Supporting Information **Figure S5**.

249 *Blood CORT release*

250 The two-way ANOVA indicated no significant effect of Group ($F_{2,17} = 0.13$; $p > 0.8$), a significant
251 effect of Time ($F_{1,17} = 235.76$; $p < 0.0001$), and no interaction between the two factors ($F_{2,17} = 0.21$;
252 $p > 0.8$) (**Figure 2**). This indicates that whereas the restraint procedure was indeed stressful, leading
253 to a marked increase of CORT release, LHb inactivation had no impact on such response, although
254 a ceiling effect remains a possibility.

255 *c-Fos+ cell densities*

256 c-Fos expression was high in almost all structures in restraint groups but also in the HC hM4-CNO
257 group (**Figure 3A**; see also Supporting Information **Table S5** for the raw data and **Tables S6** and
258 **S7** for statistics).

259 The restraint-induced increase in c-Fos expression was evidenced by significant Condition effect in
260 almost all structures at the exception of the dIS, vIS, dCA2, MD, MM, SNc, SNr, and LDT; in the
261 latter, a significant Group effect due to higher c-Fos+ cells density in the hM4-CNO group than in
262 both control groups was observed in the dIS, vIS, MD, and MM, and a significant interaction without
263 main effects of each factor due to a higher c-Fos+ cells density in the hM4-CNO-RS group than in
264 the PBS-CNO group of the same condition ($p < 0.05$) in dCA2. In regions showing activation upon
265 restraint, the analyses showed a significant Group effect - also due to higher c-Fos+ cells density in
266 hM4-CNO group compared to the two control groups which did not differ- in the PRL, LO, VO, MCC,
267 Ins_R, Ins_C, Cl, RS, vmS, PV, LS, TS, BA, CeA, dCA3, PVT, Re, and tVTA; in the LH the ANOVA
268 also indicated a significant interaction due to higher c-Fos expression in hM4-CNO-HC group as
269 compared to both HC control groups ($p < 0.001$ for each comparison). The lack of difference between
270 the (PBS or hM4)-Veh and PBS-CNO groups indicates that the effects observed in the hM4-CNO
271 group are specific to the action of CNO on hM4(Gi) receptors. However, in the LS, the Group effect
272 was also due to lower c-Fos+ cells density in PBS-CNO and, in the RD, it was only due to lower c-
273 Fos+ cells density in PBS-CNO group than the others, suggesting that CNO was not devoid of effects
274 in our conditions albeit in only a few regions. In both LHb subdivisions (**Figure 3B-C**), the ANOVA
275 indicated significant effects of Condition (LHbL: $F_{1,32} = 25.44$, $p < 0.00001$; LHbM: $F_{1,32} = 43.003$, p
276 < 0.00001) and Group (LHbL: $F_{2,32} = 14.103$, $p < 0.0001$; LHbM: $F_{1,32} = 32.414$, $p < 0.000001$) and a
277 significant interaction between both factors (LHbL: $F_{2,32} = 3.39$, $p < 0.05$; LHbM: $F_{2,32} = 4.37$, $p <$
278 0.05). The most striking findings are: in both control groups [(PBS or hM4)-Veh and PBS-CNO],
279 restraint induced c-Fos expression only in the LHbM [(PBS or hM4)-Veh, $p < 0.05$; PBS-CNO, $p <$

280 0.05], whereas in the hM4-CNO group restraint induced a significant increase in c-Fos expression
281 not only in the LHbM ($p < 0.001$) but also in the LHbL ($p < 0.001$); in the HC condition, c-Fos
282 expression was higher in the LHbM of the hM4-CNO group in comparison to both control groups (p
283 < 0.05 for each comparison). These results confirm that stress induces activation predominantly of
284 the medial subdivision of the LHb as already shown in the literature (e.g. Chastrette et al., 1991;
285 Wirtshafter et al., 1994; Brown and Shepard, 2013; Durieux et al., 2020). They also surprisingly show
286 a marked increased activation the LHb of both hM4-CNO groups. To investigate this, we performed
287 fluorescent immunohistochemical staining of the c-Fos protein and performed counting of the
288 number of cells presenting c-Fos+ or/and mCherry+ staining within the LHb. Results are presented
289 in **Figure 3D-F** and show that there are very few cells presenting a co-staining of both c-Fos and
290 mCherry in comparison with c-Fos+ or mCherry+ cells; indeed, the percentage of mCherry+ cells
291 that are also c-Fos+ is 0.87 +/- 0.19 % in the hM4-CNO-HC group and 1.46 +/- 0.44 % in the hM4-
292 CNO-RS group, and the percentage of c-Fos+ cells that are mCherry negative is 97.10 +/- 0.33 %
293 in the hM4-CNO-HC group and 97.98 +/- 0.74 % in the hM4-CNO-RS group, demonstrating that
294 DREADDed neurons and c-Fos+ neurons were mainly two segregated populations. Such an
295 increased activation of non-DREADDed neurons of the structure could reflect feedback mechanisms
296 from structures downstream to the LHb and influenced by it.

297 ***Functional Network activated by Restraint in (PBS or hM4)-Veh-RS animals***

298 We first investigated if the LHb had a significant position within the stress response control network
299 coming out of the analysis in animals not exposed to CNO, i.e., in (PBS or hM4)-Veh-RS rats. To
300 this purpose, we first calculated the correlation matrix including correlations between all structures,
301 as an estimation of functional connectivity (**Figure 4A**). This highlighted several interesting
302 correlations. For example, we found high connectivity within local networks, such as the mPFC, the
303 AMG and the midbrain monoaminergic regions. This makes perfect sense because those structures
304 are largely described to be crucial in the stress response. We also found high correlations between
305 structures of those different networks, suggesting covariation of activities of cortical, amygdalar and
306 monoaminergic structures upon stress. In other important point looking at the correlation matrix, is
307 that it presents these pools of structures jointly varying called modules. These modules represent
308 complex and robust networks. To test the randomness of these modules, we compared using
309 classical bootstrap (resampled with replacement – 500 repetitions) the (PBS or hM4)-Veh-RS matrix
310 with random matrices created from the bootstrapped (PBS or hM4)-Veh-RS matrices. The
311 comparison of the modularity of both matrices shows a significantly lower modularity coefficient in
312 the random matrix than in the initial data (bootstrap, $p < 0.05$; **Figure 4B**), suggesting that the
313 modularity observed is not random; this allows us to investigate the composition of the different
314 modules and the inter-structural interactions (see later).

315 Furthermore, we identified hubs of connectivity in this network following calculation of the strength
316 of each structure (**Figure 4C**); those key structures include: the Ins_C, the BLA, the PRh, the PVH,

317 the LH, the mBNST, the VTA, the vIS, and the PVT. The analysis indicates that these structures are
318 those including the highest density of shared connections within the network, suggesting that a large
319 part of the flow of information that passes within the network during stress exposure transits through
320 those structures. If we go further in the analysis, the 10 next structures which show a smaller – but
321 still significant – amount of connections, include structures known for their implication in the stress
322 response, such as the anterior and mid cingulate cortices, the dorsal hippocampus (dCA1 and dDG),
323 and monoaminergic regions, *i.e.*, the dopaminergic SNc and noradrenergic LC. According to our
324 main structure of interested, the LHb, whereas its medial subdivision (LHbM) is situated in the medial
325 portion of the graph, making it a hub of medium importance, the LHbL is the last structure that comes
326 out, suggesting it is a very weak actor in the stress response. Significant correlation (Pearson; $p <$
327 0.05) are represented on a graph theory network (**Figure 5**). In this network, showing the functional
328 connectivity shared by the structures investigated, we can again notice a large network which is
329 mainly supported by cortical areas (at the exception of the orbitofrontal cortex), the extended
330 amygdala and some thalamic and hypothalamic regions, such as the periventricular nuclei.

331 To better understand the place of the LHb within the network, we focused our analysis on its
332 correlations with the rest of it (**Figure 6A**). We found several significant correlations ($p < 0.05$ for
333 each association, $R^2 > 0.81$) with the entire mPFC (ACC; PRL; IL), the LS, and the MHb. As those
334 regions directly project onto the LHb, these results suggest that during stress exposure the LHb
335 process selective information directly coming from those areas. Knowing that the network is
336 composed of non-random modules, we calculated the probability of two structures to be in the same
337 modules across bootstrap repetitions (500 iterations), considering each possible pair of structures
338 (allegiance); further, we focused on the composition of the module that includes the LHbM, as well
339 as the position of this structures within the module.

340 The allegiance heatmap displayed three modules, also called “communities” (**Figure 6B**). The
341 community including the LHbM also contained the whole mPFC (ACC, PRL, IL), the Ins_C, the Ent,
342 the PRh, the LS, the TS, both lateral and medial subdivisions of the BNST, the whole AMG, the PVT,
343 the LH, the PVH, the MM, the RD, and the VTA. The community within-module strength Z-score,
344 provides the strength of the connections that a given structure shares with structures of the same
345 community or with structures of other communities (*i.e.*, strong positive scores represent high
346 interaction with structures of the same community, and strong negative scores represent high
347 interaction with structures of other communities, whereas scores around 0 indicate potential bi-
348 directional interactions, intra- and extra-community) (**Figure 6C**). Community n°1, which includes
349 the LHbM, presents an unbalanced pattern of intra/extra community interactions; indeed, only two
350 structures, the IBNST and the RD, seem to connect with structures of different communities, whereas
351 the other structures seem to either show a preference for internal communication or do not show
352 any preference. Communities n°2 and n°3 display a more balanced pattern; around half of the
353 structures promote intra-community interactions, the other half promoting extra-community

354 interactions. Interestingly, the structures present in the same community than the LHbM are crucial
355 for the stress response, i.e., the PVH, the PRL, the mBNST, the ACC, and the LA; moreover, they
356 seem to preferentially display intra-community interaction, suggesting they promote a loop for
357 information processing inside their own community. On the other hand, the IBNST and the RD could
358 be seen as input and/or output structures, as they interact with other communities although we
359 cannot know the directionality of these interactions, whether they receive information from other
360 communities to transmit them to their own, or whether they transmit information from their own
361 community to others. According to the LHbM, its within module strength z-scores – near 0 – suggests
362 it could have a role covering this of the other structures of the community, participating to intra-
363 community interactions and/or to communication with other communities either as an input or an
364 output structure.

365 ***Effects of CNO on functional connectivity***

366 The observation of the correlation matrices of the (PBS or hM4)-Veh-RS and the PBS-CNO-RS
367 groups (**Figure 7A-B**) suggested a decreased functional connectivity in the Ctl-CNO-RS group
368 (**Figure 7B**: colors are globally lighter), although cortical areas (**Figure 7B** top left purple color)
369 display a higher intra-correlation state, suggesting a hypersynchrony of those cortical networks. We
370 then evaluated the strength difference between both (PBS or hM4)-Veh-RS and PBS-CNO-RS
371 networks (**Figure 7C**) and found that some structures showed a significantly higher strength within
372 the (PBS or hM4)-Veh-RS group (classical bootstrap $p < 0.05$ and permutation test $p < 0.05$; ACC,
373 dIS, TS, PVT, LH, PVH, VTA), than within the PBS-CNO-RS group. These results suggest CNO on
374 its own might have altered the brain's functional network so that it might be difficult to evaluate the
375 net effect of the DREADD-induced LHb inactivation.

376 We also investigated the potential effect of CNO based on the stress response control network
377 (represented by the network of the (PBS or hM4)-Veh-RS group), meaning on the strength of the
378 initial communities [communities extracted from the (PBS or hM4)-Veh-RS group]. Accordingly, the
379 correlation matrix of the PBS-CNO-RS group has been sorted according to the structural
380 configuration of the communities of the (PBS or hM4)-Veh-RS group. We were able to visually notice
381 the disruption of (PBS or hM4)-Veh-RS communities in the PBS-CNO-RS group (**Figure 8A** right).
382 In addition, the evaluation of community strength across both networks [(PBS or hM4)-Veh-RS and
383 PBS-CNO-RS] showed that community n°1 and community n°3 were affected by CNO; indeed, the
384 presence of CNO decreased the strength of both communities in comparison with the (PBS or hM4)-
385 Veh group (Mann-Whitney non-parametric test; (PBS or hM4)-Veh-RS vs. PBS-CNO-RS for each
386 community; $p < 0.05$; **Figure 8B**). The fact that community n°1, which contains some of the main
387 structures implicated in the stress responses, has a lower strength in the PBS-CNO-RS network,
388 further strengthens the view that this response may have been altered by the presence of CNO.

389

390

391 **Effects of LHb inactivation on functional connectivity**

392 The observation of the correlation matrices of the PBS-CNO-RS and hM4-CNO-RS groups suggests
393 that the heatmaps of both groups are not identical but very similar (**Figure 9A**). We found several
394 significant differences regarding the strength of the structures between the (PBS or hM4)-Veh-RS
395 and PBS-CNO-RS and hM4-CNO-RS, but no difference between the PBS-CNO-RS and the hM4-
396 CNO-RS groups (see Supporting Information **Table S8**), suggesting that the strengths within the
397 network may mainly be the consequence of CNO itself, masking the effects of LHb inactivation. The
398 hM4-CNO-RS group had a quite similar community correlation heatmap than the PBS-CNO group
399 when arranged according to PBS-CNO-RS communities (**Figure 9B**). The allegiance analysis
400 detected three communities in the PBS-CNO-RS group (see Supporting Information, Composition
401 of the communities for each group). The calculation of the average strength of the communities
402 revealed that the strength of community n°1 and n°2 was significantly higher in hM4-CNO-RS group
403 than in PBS-CNO-RS ($p < 0.05$; **Figure 9C**), supporting the idea of an increased community
404 synchrony in animals with LHb inactivation.

405 In addition, we have extracted the composition of the communities of each group in order to compare
406 them (after was checked their “non-randomness” and was calculated their allegiance matrices; see
407 Supporting Information **Figure S6-8**). We calculated the Jaccard coefficient for every possible pair
408 of communities [(PBS or hM4)-Veh-RS vs PBS-CNO-RS, **Figure 10A**; PBS-CNO-RS vs hM4-CNO-
409 RS, **Figure 10B**; details on the composition of each community of each group is given at the end of
410 the Supporting Information]. The composition of the communities of the (PBS or hM4)-Veh-RS group
411 does not show much difference with this of the PBS-CNO group. For example, communities n°1 and
412 n°3 of the (PBS or hM4)-Veh-RS group network are best represented by community n°1 of the PBS-
413 CNO-RS group network (31.4 % and 31.6 % respectively). This suggests that communities n°1 and
414 3 of the (PBS or hM4)—Veh-RS group have been shuffled in the PBS-CNO-RS group, leading to a
415 reorganization of the balance between the initial communities [i.e. the communities of the (PBS or
416 hM4)-Veh-RS group, based on the original assumption that CNO should not have had any effect and
417 that communities of the PBS-CNO group should have been the same than those of the (PBS or
418 hM4)-Veh-RS group] under the influence of CNO. Also, there are more correspondences when
419 comparing communities of the PBS-CNO-RS and hM4-CNO-RS groups. For example, community
420 n°1 of the PBS-CNO-RS group is highly represented in community n°2 of the hM4-CNO-RS group
421 (47.1 %), suggesting that a large part of the consequences of LHb inactivation on the functional
422 network engaged in the stress response might be due to CNO itself. These results can be used as
423 another indication of the non-negligible consequences of CNO administration.

424

425 **DISCUSSION**

426 Restraint has extensively been used in the literature as a model of acute stress (Paré and Glavin,
427 1986). The increased plasmatic CORT concentration observed in all groups seems to validate, if
428 needed, this stressful procedure, as it stimulates the HPA axis. The lack of impact of LHb inactivation
429 on CORT release appears consistent with those already found in our laboratory, showing that LHb
430 inactivation only seems to affect CORT release when there is a cognitive task to perform (Mathis et
431 al., 2018).

432 Following restraint, we found a generalized marked increase in the density of c-Fos+ cells, indicating
433 the engagement of many different brain structures in the stress response, as expected (Herman et
434 al., 2003; Sousa, 2016). The functional network that seems to support this response possesses a
435 significant modularity (communities of structures which vary together). This modular architecture is
436 a characteristic of small world networks (i.e., a high number of short connections between structures
437 and a high level of local clustering between structures). This type of network is known to be very
438 robust to structural alterations (if one of the nodes is deleted, the information that originally should
439 have passed through this node is eventually rerouted to finally reach its destination without
440 increasing too much the distance it travelled; Sporns et al. 2004; Bassett and Bullmore 2006; Stam
441 and Reijneveld 2007; Reijneveld et al. 2007). Small world architectures are known to be robust
442 networks, promoting rapid information transfer and network synchronization, and providing efficient
443 balance between global integration and local processing (Sporns, 2013). Accordingly, the network
444 engaged upon restraint may be very plastic and robust permitting a very integrated balance of local
445 and global processing leading to highly efficient information transfer at low energy cost.

446 We found the principal hubs of the stress response network to be the Ins_C, the BA and the PVH,
447 which are main components of the stress response network. The Ins is associated with the
448 modulation of the autonomic response, including somatosensory, nociceptive and visceral
449 processing (Kimura et al., 2010; Menon and Uddin, 2010; Rogers-Carter et al., 2018; Aguilar-Rivera
450 et al., 2020; Ming et al., 2020); in addition, the more caudal part of the Ins (Ins_C), which is the one
451 coming out in our analysis, is involved in respiratory and cardiovascular controls (Bagaev and
452 Aleksandrov, 2006). The engagement of the Ins_C makes perfect sense as the autonomic response
453 facing stress is crucial to allow efficient coping (Selye, 1950; de Kloet et al., 1998). The PVH and the
454 BA are also key structures of the stress response (Prewitt and Herman, 1998; Roozendaal et al.,
455 2009; Sousa, 2016). As said above, the PVH is the entry point of the HPA axis which triggers the
456 physiological response to a stressor through the stimulation of CORT release (Herman et al., 2003;
457 Ulrich-Lai and Herman, 2009). The BLA is essential for processing stressors (Janak and Tye, 2015);
458 it is activated by the anticipation of a stressor (Cullinan et al., 1995) and involved in the consolidation
459 of aversive memories (Roozendaal et al., 2009). Other key structures of the stress response were
460 present in the twenty first hubs that came out from the analysis, including the mBNST, the LA, the

461 mPFC (ACC, PRL), the HPC (dDG, dCA1), and the dopaminergic (SNc and VTA) and noradrenergic
462 (LC) systems (Herman et al., 2003; Sousa, 2016; Godoy et al., 2018).

463 With regard to the structure of interest of the current study, the LHb, our results first confirmed that
464 its medial part (LHbM) is preferentially activated by stress (Chastrette et al., 1991; Wirtshafter et al.,
465 1994; Brown and Shepard, 2013; Durieux et al., 2020). The LHbM has long been referred to as the
466 “limbic” subdivision of the LHb, as it is directly connected with the mPFC, but also with the
467 hypothalamus and the monoamine systems (Metzger et al., 2021). It therefore makes perfect sense
468 that in the subsequent community analyses of the (PBS or hM4)-Veh-RS group we found strong
469 correlation between the LHbM and the mPFC (ACC, PRL and IL). In addition, we found the LHbM to
470 be significantly correlated to the LS and the MHb. The proximity with the LS is not surprising as
471 identical correlation has been demonstrated using PET + 18-FDG in rats exposed to inescapable
472 foot-shocks (Mirrione et al., 2014). The link with the MHb is more surprising but very interesting.
473 Surprising because the current view is generally that the LHb and the MHb are distinct in terms of
474 anatomical connections and functions; first of all, although the two habenular subregions are indeed
475 very distinct in terms of input and output connections, Kim and Chang (2005) have described a small
476 subset of MHb neurons making en passant synapses on dendrites of LHb neurons before exiting the
477 MHb by the fasciculus retroflexus, suggesting that both regions can share information; these
478 information can indeed be related to the stress response as molecular mechanisms within the MHb
479 have recently been involved in despair-like behavior in mice (Yoo et al., 2021) whereas c-Fos
480 expression was found to be increased in the MHb in rats susceptible to chronic mild stress (Febbraro
481 et al., 2017). These different results imply that both the LHb and MHb could conjointly participate to
482 stress-related responses, such as suggested by our own findings.

483 Community analyses revealed that, in addition to the mPFC, the LHbM shared strong functional
484 connections with the PVH, the Ins_C, the extended amygdala (BA, LA, CeA, BNST), and the
485 dopamine (VTA) and serotonin (RD) systems. These results support the view that the LHb receives
486 and integrates information from several macrosystems (Geisler and Trimble, 2008), including cortical
487 and amygdalar, related to several aspects of the stress response, and that it could represent a relay
488 of those information towards the monoaminergic centers (VTA and RD), which are engaged in the
489 control of the activity of cortical and subcortical structures to favor coping.

490 An important result of our study that should be highlighted for future studies is the unexpected effect
491 of CNO on the stress network. Behavioral effects of CNO have generally been observed following
492 administration of doses of CNO higher than the one we used (Manvich et al., 2018), while the vast
493 majority of the studies did not report any adverse behavioral consequences following CNO
494 administration (e.g., Aponte et al., 2011; Ferguson et al., 2013; Augur et al., 2016; Han et al., 2017;
495 Durieux et al., 2020). Our analyses demonstrate an undeniable effect of CNO as correlation matrices
496 of (PBS or hM4)-Veh-RS and PBS-CNO-RS groups considerably differ. Because in our protocol
497 CNO was injected 30 min before restraint, this can suggest the integrity of the stress response

498 network “to be engaged” during restraint had been compromised in rats of the group including LHB
499 inactivation. These effects are probably related to the metabolism of CNO into clozapine (Gomez et
500 al., 2017; Manvich et al., 2018), a psychoactive compound which can influence many
501 neurotransmitter systems through its action on dopamine (D1 and D4), serotonin (including 5HT1A
502 and 5HT2A), noradrenaline (alpha 1 and 2), histamine (H1), and muscarinic (M1, M3 and M4)
503 receptors (Aringhieri et al., 2018). Importantly, in HC condition, CNO did not induce c-Fos expression
504 in all the brain areas known to be activated by clozapine like the mPFC and the NAc (see e.g.,
505 Robertson and Fibiger, 1992); this suggests that although CNO was converted into clozapine, its
506 level was probably too low to induce a generalized effect. However, even if CNO altered the level of
507 c-Fos expression in only a few regions, network analyses indicated a lower strength of many
508 structures following its administration, including the ACC, the PVH, and the VTA. We can therefore
509 hypothesize that the detrimental effects of CNO on the organization of the network came from the
510 perturbation of the modulatory function of the HPA axis and of the dopamine system, two very
511 important modulators of the physiological stress response. Interestingly, in rats, at the same
512 concentration we used (1 mg/kg), CNO reduced the acoustic startle reflex (MacLaren et al., 2016)
513 and induced interoceptive effects that partially substitute to that of a low dose of clozapine (Manvich
514 et al., 2018), suggesting it can affect components of the stress response. In trying to differentiate
515 between the effects of CNO itself and the consequences of LHB inactivation, we could only observe
516 that even if some communities were showing some differences between both conditions, the
517 interactions within the communities of the two groups remained quite similar, suggesting the effect
518 of LHB inactivation had been partly masked by the effects of CNO. Finally, it is to be reminded here
519 that control animals were injected with PBS (or the DREADD viral vector in the case of Veh control
520 groups) and not the usual control vector (i.e. AAV-CAMKII-mCherry). Therefore, our results must be
521 considered with this in mind, although to our knowledge detrimental behavioural consequences have
522 never been reported following the injection of a DREADD control vector.

523 **CONCLUSIONS**

524 We have seen that the LHB, and more specifically its medial subdivision, the LHbM, was engaged,
525 during acute stress exposure, among a broad network of key regions of the stress response. Given
526 its anatomical position, the role of the LHbM could be to integrate multiple stress-related information
527 stemming in cortical, thalamic and hypothalamic regions to further communicate it downstream to
528 monoaminergic systems in order to probably initiate coping strategies. As shown by others, the LHB
529 – or its equivalent in zebrafishes – is engaged in behavioral adaptation under stressful situations
530 (Ootsuka and Mohammed, 2015; Berger et al., 2018; Andalman et al., 2019; Coffey et al., 2020).
531 Better understanding the engagement of the LHB when individuals are exposed to stressful situation
532 appears like a relevant question as alteration of LHB function or morphology has been evidenced in
533 stress-related psychiatric pathologies such as depression (Browne et al., 2018; Gold and Kadriu,

534 2019; Hu et al., 2020) and schizophrenia (Sandyk, 1992; Shepard et al., 2006; Zhang et al., 2017;
535 but see Schafer et al., 2018).
536

REFERENCES

- Aguilar-Rivera, M., Kim, S., Coleman, T.P., Maldonado, P.E., Torrealba, F. (2020). Interoceptive insular cortex participates in sensory processing of gastrointestinal malaise and associated behaviors. *Sci Rep*, **10**, 21642.
- Aizawa, H., Yanagihara, S., Kobayashi, M., Niisato, K., Takekawa, T., Harukuni, R., McHugh, T.J., Fukai, T., Isomura, Y., Okamoto, H. (2013). The synchronous activity of lateral habenular neurons is essential for regulating hippocampal theta oscillation. *J Neurosci*, **33**, 8909-21.
- Ali, M., Cholvin, T., Muller, M.A., Cosquer, B., Kelche, C., Cassel, J.-C., Pereira de Vasconcelos, A. (2017). Environmental enrichment enhances systems-level consolidation of a spatial memory after lesions of the ventral midline thalamus. *Neurobiol Learn Mem*, **141**, 108–123.
- Andalman, A.S., Burns, V.M., Lovett-Barron, M., Broxton, M., Poole, B., Yang, S.J., Grosenick, L., Lerner, T.N., Chen, R., Benster, T., Mourrain, P., Levoy, M., Rajan, K., Deisseroth, K. (2019). Neuronal Dynamics Regulating Brain and Behavioral State Transitions. *Cell*, **177**, 970-985.
- Aponte, Y., Atasoy, D., Sternson, S.M. (2011). AGRP neurons are sufficient to orchestrate feeding behavior rapidly and without training. *Nat Neurosci*, **14**, 351–355.
- Aringhieri, S., Carli, M., Kolachalam, S., Verdesca, V., Cini, E., Rossi, M., McCormick, P.J., Corsini, G.U., Maggio, R., Scarselli, M. (2018). Molecular targets of atypical antipsychotics: From mechanism of action to clinical differences. *Pharmacol Ther*, **192**, 20–41.
- Augur, I.F., Wyckoff, A.R., Aston-Jones, G., Kalivas, P.W., Peters, J. (2016). Chemogenetic Activation of an Extinction Neural Circuit Reduces Cue-Induced Reinstatement of Cocaine Seeking. *J Neurosci*, **36**, 10174–10180.
- Bagaev, V., Aleksandrov, V. (2006). Visceral-related area in the rat insular cortex. *Auton Neurosci Basic Clin*, **125**, 16–21.
- Baker, P.M., Rao, Y., Rivera, Z.M.G., Garcia, E.M., Mizumori, S.J.Y. (2019). Selective Functional Interaction Between the Lateral Habenula and Hippocampus During Different Tests of Response Flexibility. *Front Mol Neurosci*, **12**, 245.
- Bankhead, P., Loughrey, M.B., Fernández, J.A., Dombrowski, Y., McArt, D.G., Dunne, P.D., McQuaid, S., Gray, R.T., Murray, L.J., Coleman, H.G., James, J.A., Salto-Tellez, M., Hamilton, P.W. (2017). QuPath: Open source software for digital pathology image analysis. *Sci Rep*, **7**, 16878.
- Barrett, D.W., Gonzalez-Lima, F. (2018). Prefrontal-limbic Functional Connectivity during Acquisition and Extinction of Conditioned Fear. *Neuroscience*, **376**, 162–171.
- Bassett, D.S., Bullmore, E. (2006). Small-world brain networks. *Neurosci Rev J Bringing Neurobiol Neurol Psychiatry*, **12**, 512–523.
- Berger, A.L., Henricks, A.M., Lugo, J.M., Wright, H.R., Warrick, C.R., Sticht, M.A., Morena, M., Bonilla, I., Laredo, S.A., Craft, R.M., Parsons, L.H., Grandes, P.R., Hillard, C.J., Hill, M.N., McLaughlin, R.J. (2018). The Lateral Habenula Directs Coping Styles Under Conditions of Stress via Recruitment of the Endocannabinoid System. *Biol Psychiatry*, **84**, 611-623.
- Brown, P.L., Shepard, P.D. (2013). Lesions of the fasciculus retroflexus alter footshock-induced cFos expression in the mesopontine rostromedial tegmental area of rats. *PLoS One*, **8**, e60678.
- Browne, C.A., Hammack, R., Lucki, I. (2018). Dysregulation of the Lateral Habenula in Major Depressive Disorder. *Front Synaptic Neurosci*, **7**, 10:46.
- Bullmore, E., Sporns, O. (2009). Complex brain networks: graph theoretical analysis of structural and functional systems. *Nat Rev Neurosci*, **10**, 186–198.

- Cenci, M.A., Kalén, P., Mandel, R.J., Björklund, A. (1992). Regional differences in the regulation of dopamine and noradrenaline release in medial frontal cortex, nucleus accumbens and caudate-putamen: a microdialysis study in the rat. *Brain Res*, **581**, 217-28.
- Chastrette, N., Pfaff, D.W., Gibbs, R.B. (1991). Effects of daytime and nighttime stress on Fos-like immunoreactivity in the paraventricular nucleus of the hypothalamus, the habenula, and the posterior paraventricular nucleus of the thalamus. *Brain Res*, **563**, 339–344.
- Christoph, G.R., Leonzio, R.J., Wilcox, K.S. (1986). Stimulation of the lateral habenula inhibits dopamine-containing neurons in the substantia nigra and ventral tegmental area of the rat. *J Neurosci*, **6**, 613-9.
- Coffey, K.R., Marx, R.G., Vo, E.K., Nair, S.G., Neumaier, J.F. (2020). Chemogenetic inhibition of lateral habenula projections to the dorsal raphe nucleus reduces passive coping and perseverative reward seeking in rats. *Neuropsychopharmacol Off Publ Am Coll Neuropsychopharmacol*, **45**, 1115–1124.
- Cullinan, W.E., Herman, J.P., Battaglia, D.F., Akil, H., Watson, S.J. (1995). Pattern and time course of immediate early gene expression in rat brain following acute stress. *Neuroscience*, **64**, 477–505.
- de Kloet, E.R., Vreugdenhil, E., Oitzl, M.S., Joëls, M. (1998). Brain Corticosteroid Receptor Balance in Health and Disease. *Endocr Rev*, **19**, 269–301.
- Derman, R.C., Bass, C.E., Ferrario, C.R. (2020). Effects of hM4Di activation in CamKII basolateral amygdala neurons and CNO treatment on sensory-specific vs. general PIT: refining PIT circuits and considerations for using CNO. *Psychopharmacology (Berl)*, **237**, 1249–1266.
- Dolzani, S.D., Baratta, M.V., Amat, J., Agster, K.L., Saddoris, M.P., Watkins, L.R., Maier, S.F. (2016). Activation of a Habenulo-Raphe Circuit Is Critical for the Behavioral and Neurochemical Consequences of Uncontrollable Stress in the Male Rat. *eNeuro*, **3**.
- Dong, H.W., Swanson, L.W. (2004). Organization of axonal projections from the anterolateral area of the bed nuclei of the stria terminalis. *J Comp Neurol*, **468**, 277-98.
- Dong, H.W., Swanson, L.W. (2006). Projections from bed nuclei of the stria terminalis, dorsomedial nucleus: implications for cerebral hemisphere integration of neuroendocrine, autonomic, and drinking responses. *J Comp Neurol*, **494**, 75-107.
- Durieux, L., Mathis, V., Herbeaux, K., Muller, M.-A., Barbelivien, A., Mathis, C., Schlichter, R., Hugel, S., Majchrzak, M., Lecourtier, L. (2020). Involvement of the lateral habenula in fear memory. *Brain Struct Funct*, **225**, 2029-2044.
- Febbraro, F., Svenningsen, K., Tran, T.P., Wiborg, O. (2017). Neuronal substrates underlying stress resilience and susceptibility in rats. *PLoS One*, **12**, e0179434.
- Ferguson, S.M., Phillips, P.E.M., Roth, B.L., Wess, J., Neumaier, J.F. (2013). Direct-Pathway Striatal Neurons Regulate the Retention of Decision-Making Strategies. *J Neurosci*, **33**, 11668–11676.
- Geisler, S., Trimble, M. (2008). The Lateral Habenula: No Longer Neglected. *CNS Spectr*, **13**, 484–489.
- Godoy, L.D., Rossignoli, M.T., Delfino-Pereira, P., Garcia-Cairasco, N., de Lima Umeoka, E.H. (2018). A Comprehensive Overview on Stress Neurobiology: Basic Concepts and Clinical Implications. *Front Behav Neurosci*, **12**, 127.
- Gold, P.W., Kadriu, B. (2019). A Major Role for the Lateral Habenula in Depressive Illness: Physiologic and Molecular Mechanisms. *Front Psychiatry*, **10**, 320.

- Gomez, J.L., Bonaventura, J., Lesniak, W., Mathews, W.B., Sysa-Shah, P., Rodriguez, L.A., Ellis, R.J., Richie, C.T., Harvey, B.K., Dannals, R.F., Pomper, M.G., Bonci, A., Michaelides, M. (2017). Chemogenetics revealed: DREADD occupancy and activation via converted clozapine. *Science*, **357**, 503–507.
- González-Pardo, H., Conejo, N.M., Lana, G., Arias, J.L. (2012). Different brain networks underlying the acquisition and expression of contextual fear conditioning: a metabolic mapping study. *Neuroscience*, **202**, 234–242.
- Goutagny, R., Loureiro, M., Jackson, J., Chaumont, J., Williams, S., Isope, P., Kelche, C., Cassel, J.C., Lecourtier, L. (2013). Interactions between the lateral habenula and the hippocampus: implication for spatial memory processes. *Neuropsychopharmacology*, **38**, 2418–26.
- Han, S., Yang, S.H., Kim, J.Y., Mo, S., Yang, E., Song, K.M., Ham, B.-J., Mechawar, N., Turecki, G., Lee, H.W., Kim, H. (2017). Down-regulation of cholinergic signaling in the habenula induces anhedonia-like behavior. *Sci Rep*, **7**, 900.
- Henckens, M.J.A.G., van der Marel, K., van der Toorn, A., Pillai, A.G., Fernández, G., Dijkhuizen, R.M., Joëls, M. (2015). Stress-induced alterations in large-scale functional networks of the rodent brain. *NeuroImage*, **105**, 312–322.
- Herman, J.P., Figueiredo, H., Mueller, N.K., Ulrich-Lai, Y., Ostrander, M.M., Choi, D.C., Cullinan, W.E. (2003). Central mechanisms of stress integration: hierarchical circuitry controlling hypothalamo–pituitary–adrenocortical responsiveness. *Front Neuroendocrinol*, **24**, 151–180.
- Hikosaka, O. (2010). The habenula: from stress evasion to value-based decision-making. *Nat Rev Neurosci*, **11**, 503–513.
- Hu, H., Cui, Y., Yang, Y. (2020). Circuits and functions of the lateral habenula in health and in disease. *Nat Rev Neurosci*, **21**, 277–295.
- Hudson, A.E. (2018). Genetic Reporters of Neuronal Activity: c-Fos and G-CaMP6. *Methods Enzymol*, **603**, 197–220.
- Jacinto, L.R., Mata, R., Novais, A., Marques, F., Sousa, N. (2017). The habenula as a critical node in chronic stress-related anxiety. *Exp Neurol*, **289**, 46–54.
- Janak, P.H., Tye, K.M. (2015). From circuits to behaviour in the amygdala. *Nature*, **517**, 284–292.
- Ji, H., Shepard, P.D. (2007). Lateral habenula stimulation inhibits rat midbrain dopamine neurons through a GABA(A) receptor-mediated mechanism. *J Neurosci*, **27**, 6923–30.
- Joëls, M., Baram, T.Z. (2009). The neuro-symphony of stress. *Nat Rev Neurosci*, **10**, 459–466.
- Kalén, P., Lindvall, O., Björklund, A. (1989a). Electrical stimulation of the lateral habenula increases hippocampal noradrenaline release as monitored by in vivo microdialysis. *Exp Brain Res*, **76**, 239–45.
- Kalén, P., Strecker, R.E., Rosengren, E., Björklund, A. (1989b). Regulation of striatal serotonin release by the lateral habenula-dorsal raphe pathway in the rat as demonstrated by in vivo microdialysis: role of excitatory amino acids and GABA. *Brain Res*, **492**, 187–202.
- Kim, U., Chang, S.-Y. (2005). Dendritic morphology, local circuitry, and intrinsic electrophysiology of neurons in the rat medial and lateral habenular nuclei of the epithalamus. *J Comp Neurol*, **483**, 236–250.
- Kim, U., Lee, T. (2012). Topography of descending projections from anterior insular and medial prefrontal regions to the lateral habenula of the epithalamus in the rat. *Eur J Neurosci*, **35**, 1253–69.

- Kimura, A., Imbe, H., Donishi, T. (2010). Efferent connections of an auditory area in the caudal insular cortex of the rat: anatomical nodes for cortical streams of auditory processing and cross-modal sensory interactions. *Neuroscience*, **166**, 1140–1157.
- Kovács, K.J. (1998). Invited review c-Fos as a transcription factor: a stressful (re)view from a functional map. *Neurochem Int*, **33**, 287–297.
- Lammel, S., Lim, B.K., Ran, C., Huang, K.W., Betley, M.J., Tye, K.M., Deisseroth, K., Malenka, R.C. (2012). Input-specific control of reward and aversion in the ventral tegmental area. *Nature*, **491**, 212–217.
- Lecca, S., Truscel, M., Mameli, M. (2017). Footshock-induced plasticity of GABAB signalling in the lateral habenula requires dopamine and glucocorticoid receptors. *Synapse*, **71**.
- Lecourtier, L., Defrancesco, A., Moghaddam, B. (2008). Differential tonic influence of lateral habenula on prefrontal cortex and nucleus accumbens dopamine release. *Eur J Neurosci*, **27**, 1755–62.
- MacLaren, D.A.A., Browne, R.W., Shaw, J.K., Krishnan Radhakrishnan, S., Khare, P., España, R.A., Clark, S.D. (2016). Clozapine N-Oxide Administration Produces Behavioral Effects in Long-Evans Rats: Implications for Designing DREADD Experiments. *eNeuro*, **3**.
- Magalhães, R., Barrière, D.A., Novais, A., Marques, F., Marques, P., Cerqueira, J., Sousa, J.C., Cachia, A., Boumezbear, F., Bottlaender, M., Jay, T.M., Mériaux, S., Sousa, N. (2018). The dynamics of stress: a longitudinal MRI study of rat brain structure and connectome. *Mol Psychiatry*, **23**, 1998–2006.
- Manvich, D.F., Webster, K.A., Foster, S.L., Farrell, M.S., Ritchie, J.C., Porter, J.H., Weinschenker, D. (2018). The DREADD agonist clozapine N-oxide (CNO) is reverse-metabolized to clozapine and produces clozapine-like interoceptive stimulus effects in rats and mice. *Sci Rep*, **8**.
- Mathis, V., Cosquer, B., Barbelivien, A., Herbeaux, K., Bothorel, B., Sage-Ciocca, D., Poirel, V.-J., Mathis, C., Lecourtier, L. (2018). The lateral habenula interacts with the hypothalamo-pituitary adrenal axis response upon stressful cognitive demand in rats. *Behav Brain Res*, **341**, 63–70.
- McEwen, B.S., Bowles, N.P., Gray, J.D., Hill, M.N., Hunter, R.G., Karatsoreos, I.N., Nasca, C. (2015). Mechanisms of stress in the brain. *Nat Neurosci*, **18**, 1353–1363.
- Menon, V., Uddin, L.Q. (2010). Saliency, switching, attention and control: a network model of insula function. *Brain Struct Funct*, **214**, 655–667.
- Metzger, M., Souza, R., Lima, L.B., Bueno, D., Gonçalves, L., Segó, C., Donato, J., Shammah-Lagnado, S.J. (2021). Habenular connections with the dopaminergic and serotonergic system and their role in stress-related psychiatric disorders. *Eur J Neurosci*, **53**, 65–88.
- Ming, Q., Ma, H., Li, J., Yang, F., Li, J., Liang, J., Li, D., Lin, W. (2020). Changes in autonomic nervous function and influencing factors in a rat insular cortex electrical kindling model. *Neurosci Lett*, **721**, 134782.
- Mirrione, M.M., Schulz, D., Lapidus, K.A.B., Zhang, S., Goodman, W., Henn, F.A. (2014). Increased metabolic activity in the septum and habenula during stress is linked to subsequent expression of learned helplessness behavior. *Front Hum Neurosci*, **8**.
- Murphy, C.A., DiCamillo, A.M., Haun, F., Murray, M. (1996). Lesion of the habenular efferent pathway produces anxiety and locomotor hyperactivity in rats: a comparison of the effects of neonatal and adult lesions. *Behav Brain Res*, **81**, 43–52.

- Ootsuka, Y., Mohammed, M. (2015). Activation of the habenula complex evokes autonomic physiological responses similar to those associated with emotional stress. *Physiol Rep*, **3**, e12297.
- Ootsuka, Y., Mohammed, M., Blessing, W.W. (2017). Lateral habenula regulation of emotional hyperthermia: mediation via the medullary raphé. *Sci Rep*, **7**, 4102.
- Paré, W.P., Glavin, G.B. (1986). Restraint stress in biomedical research: a review. *Neurosci Biobehav Rev*, **10**, 339–370.
- Prewitt, C.M.F., Herman, J.P. (1998). Anatomical interactions between the central amygdaloid nucleus and the hypothalamic paraventricular nucleus of the rat: a dual tract-tracing analysis. *J Chem Neuroanat*, **15**, 173–186.
- Reijneveld, J.C., Ponten, S.C., Berendse, H.W., Stam, C.J. (2007). The application of graph theoretical analysis to complex networks in the brain. *Clin Neurophysiol*, **118**, 2317–2331.
- Reisine, T.D., Soubrié, P., Artaud, F., Glowinski, J. (1982). Involvement of lateral habenula-dorsal raphe neurons in the differential regulation of striatal and nigral serotonergic transmission cats. *J Neurosci*, **2**, 1062-71.
- Robertson, G.S., Fibiger, H.C. (1992). Neuroleptics increase C-FOS expression in the forebrain: Contrasting effects of haloperidol and clozapine. *Neuroscience*, **46**, 315–328.
- Rogers-Carter, M.M., Varela, J.A., Gribbons, K.B., Pierce, A.F., McGoey, M.T., Ritchey, M., Christianson, J.P. (2018). Insular cortex mediates approach and avoidance responses to social affective stimuli. *Nat Neurosci*, **21**, 404–414.
- Roosendaal, B., McEwen, B.S., Chattarji, S. (2009). Stress, memory and the amygdala. *Nat Rev Neurosci*, **10**, 423–433.
- Sandyk, R. (1992). Pineal and habenula calcification in schizophrenia. *Int J Neurosci*, **67**, 19-30.
- Selye, H. (1950). Stress and the General Adaptation Syndrome. *Br Med J*, **1**, 1383–1392.
- Shabel, S.J., Proulx, C.D., Trias, A., Murphy, R.T., Malinow, R. (2012). Input to the Lateral Habenula from the Basal Ganglia Is Excitatory, Aversive, and Suppressed by Serotonin. *Neuron*, **74**, 475–481.
- Schafer, M., Kim J.W., Joseph, J., Xu, J., Frangou S., Doucet G.E. (2018) Imaging Habenula Volume in Schizophrenia and Bipolar Disorder. *Front Psychiatry*, **9**, 456.
- Shepard, P.D., Holcomb, H.H., Gold, J.M. (2006). Schizophrenia in translation: the presence of absence: habenular regulation of dopamine neurons and the encoding of negative outcomes. *Schizophr Bull*, **32**, 417-21.
- Sousa, N. (2016). The dynamics of the stress neuromatrix. *Mol Psychiatry*, **21**, 302–312.
- Sporns, O. (2013). Network attributes for segregation and integration in the human brain. *Curr Opin Neurobiol*, **23**, 162–171.
- Sporns, O., Chialvo, D.R., Kaiser, M., Hilgetag, C.C. (2004). Organization, development and function of complex brain networks. *Trends Cogn Sci*, **8**, 418–425.
- Stam, C.J., Reijneveld, J.C. (2007). Graph theoretical analysis of complex networks in the brain. *Nonlinear Biomed Phys*, **1**, 3.
- Stamatakis, A.M., Stuber, G.D. (2012). Activation of lateral habenula inputs to the ventral midbrain promotes behavioral avoidance. *Nat Neurosci*, **15**, 1105–1107.

- Ulrich-Lai, Y.M., Herman, J.P. (2009). Neural regulation of endocrine and autonomic stress responses. *Nat Rev Neurosci*, **10**, 397–409.
- Vetere, G., Kenney, J.W., Tran, L.M., Xia, F., Steadman, P.E., Parkinson, J., Josselyn, S.A., Frankland, P.W. (2017). Chemogenetic Interrogation of a Brain-wide Fear Memory Network in Mice. *Neuron*, **94**, 363-374.e4.
- Wheeler, A.L., Teixeira, C.M., Wang, A.H., Xiong, X., Kovacevic, N., Lerch, J.P., McIntosh, A.R., Parkinson, J., Frankland, P.W. (2013). Identification of a functional connectome for long-term fear memory in mice. *PLoS Comput Biol*, **9**, e1002853.
- Wirtshafter, D., Asin, K.E., Pitzer, M.R. (1994). Dopamine agonists and stress produce different patterns of Fos-like immunoreactivity in the lateral habenula. *Brain Res*, **633**, 21–26.
- Yoo, H., Yang, S.H., Kim, J.Y., Yang, E., Park, H.S., Lee, S.J., Rhyu, I.J., Turecki, G., Lee, H.W., Kim, H. (2021). Down-regulation of habenular calcium-dependent secretion activator 2 induces despair-like behavior. *Sci Rep*, **11**, 3700.
- Zhang, J., Tan, L., Ren, Y., Liang, J., Lin, R., Feng, Q., Zhou, J., Hu, F., Ren, J., Wei, C., Yu, T., Zhuang, Y., Bettler, B., Wang, F., Luo, M. (2016). Presynaptic Excitation via GABAB Receptors in Habenula Cholinergic Neurons Regulates Fear Memory Expression. *Cell*, **166**, 716–728.
- Zhang, L., Wang, H., Luan, S., Yang, S., Wang, Z., Wang, J., Zhao H. (2017). Altered Volume and Functional Connectivity of the Habenula in Schizophrenia. *Front Hum Neurosci*, **11**, 636.
- Zhou W, Jin Y, Meng Q, Zhu X, Bai T, Tian Y, Mao Y, Wang L, Xie W, Zhong H, Zhang N, Luo MH, Tao W, Wang H, Li J, Li J, Qiu BS, Zhou JN, Li X, Xu H, Wang K, Zhang X, Liu Y, Richter-Levin G, Xu L, Zhang Z. (2019). A neural circuit for comorbid depressive symptoms in chronic pain. *Nat Neurosci*, **22**, 1649-1658.

FIGURES LEGENDS

FIGURE 1 **(A)** Timeline of the experiment. Rats of the present study are those of a previously published study (Durieux et al. 2020). They underwent surgery 7 to 9 weeks prior to the present experiment, and then went on several tests including elevated plus maze, fear conditioning and locomotor activity assessment. One week elapsed between the end of the previous set of experiment and the restraint procedure during which they were kept in a tube for 10 min. Controls remained in their home cage. The injection of CNO (1 mg/kg) or vehicle was performed 30 min before. In restrained animals, blood samples were collected once 2 min before and once 2 min after restraint. Eighty min following restraint, animals were deeply anesthetized, intracardiac perfusion was performed and brains were removed. Blood samples were run through a mass spectrometer to assess corticosterone levels. Brains were cut, and immunolabeling of the c-Fos protein was performed on 40 μ m-thick floating sections. The density of c-Fos+ cells was calculated in each region of interest. **(B)** Regions of interest comprised cortical (purple), basal ganglia and septal (green), extended amygdalar (pink), habenular (orange), hippocampal (yellow), thalamic and hypothalamic (grey), and brainstem (blue) regions.

FIGURE 2 Effect of restraint and LHb inactivation on CORT plasmatic concentration. Mean CORT plasmatic concentration (\pm S.E.M) before (left) and after (right) restraint in (PBS or hM4)-Veh-RS (white bars), PBS-CNO-RS (light grey bars) and hM4-CNO-RS (dark grey bars) groups (white circles represent individual values). Statistics: * $p < 0.05$ vs. pre-restraint in the same group.

FIGURE 3 Effects of restraint and LHb inactivation on c-Fos expression. **(A)** Heatmap of mean c-Fos+ density per structures for all groups. **(B)** Photography of c-Fos labeling in the entire habenula in (PBS or hM4)-Veh (top), PBS-CNO (middle), and hM4-CNO (bottom) groups in the HC (left) and RS (right) conditions. **(C)** Bar plot of c-Fos+ density (mean \pm S.E.M) in the LHbL and LHbM (circles represent individual values; for (PBS or HM4)-Veh control groups, the red circles represent individual values of rats injected with the AAV-hM4(Gi)-mCherry viral vector and white circle individual values of those injected with PBS). **(D)** Density (mean \pm S.E.M) of mCherry+, c-Fos+, and mCherry+/c-Fos+ doubly labeled neurons within the LHb of animals injected with the viral vector AAV8-CamKII-hM4(Gi)-mCherry and injected with CNO either in the HC (white bars) or in the RS (light grey bars) condition (white circles represent individual values). **(E)** Representative image of the c-Fos+ (green) and mCherry+ (red) neuronal population in the LHb of a hM4-CNO-RS (top) and a hM4-CNO-HC (bottom) rat. **(F)** Magnification of LHb neurons showing the different neuronal population such as they were observed following c-Fos immunostaining, i.e. a c-Fos+ neuron (*), a mCherry+ neuron (**), and a doubly labelled mCherry+/c-Fos+ neuron (pointed to by a white arrow). Statistics: *** $p <$

0.001 vs. all other groups; [&] $p < 0.05$ vs. the corresponding HC group; [§] $p < 0.05$ vs. the other HC groups (Newman-Keuls post-hoc test following ANOVA).

FIGURE 4 Evaluation of the network engaged by restraint. **(A)** Heatmap representing the cross-correlations (color scale, Pearson correlation R^2 ; red represent positive, and blue negative, correlations) between all investigated structures represented with a color code according to main brain regions (cortical regions, purple; basal ganglia and septum, green; extended amygdala, pink; habenula, red; hippocampus, yellow; thalamus and hypothalamus, grey; brainstem, blue). **(B)** Modularity based on Louvain algorithm, in the (PBS or hM4)-Veh-RS group and its associated random network. Statistics: bootstrap, $*p < 0.05$. **(c)** Strength of each structure in decreasing order. The ten structures (Ins_C to PVT) displaying the highest strength are represented in dark grey and the tens following in light grey.

FIGURE 5 Graphical representation of the network depicted in Figure 4a, with nodes (structures) and edges (connecting lines representing significant correlations; Pearson $p < 0.05$). Positive correlations are represented in red and negative ones in blue.

FIGURE 6 LHbM implication in the stress response may be supported by its functional connections. **(A)** Pearson correlation (R^2) between the LHbM and structures of the network. Horizontal black lines represent the threshold of significant correlations ($p < 0.05$). The structures are ordered by areas (cortical areas, purple; basal ganglia and septum, green; extended amygdala, pink; habenula, red; hippocampus, yellow; thalamus and hypothalamus, grey; brainstem, blue). Note that the correlation of the LHbM with itself equals 1. **(B)** Heatmap of allegiance of the (PBS or hM4)-Veh-RS group, representing the probability for two given structures to belong to the same community across the bootstrap iterations (the darker, the higher probability). **(C)** Within-modules strength z-score organized by structures according to the community they belong to. The communities have been detected on the allegiance matrix of the (PBS or hM4)-Veh-RS with Louvain algorithm.

FIGURE 7 Effects of CNO injection on brain functional network. Heatmap representing the cross-correlations (color scale, Pearson correlation R^2 ; red represent positive, and blue negative, correlations) between all structures organized by main regions (cortical regions, purple; basal ganglia and septum, green; extended amygdala, pink; habenula, red; hippocampus, yellow; thalamus and hypothalamus, grey; brainstem, blue) for (PBS or hM4)-Veh-RS **(A)** and PBS-CNO-RS **(B)**. **(C)** Strength difference for each structure between the (PBS or hM4)-Veh-RS group and the PBS-CNO-RS group organized by main areas (positive scores indicate a higher strength in the (PBS or hM4)-

Veh-RS group compared to PBS-CNO-RS group; negative scores indicate a higher strength in the PBS-CNO-RS than in (PBS or hM4)-Veh-RS group). Statistics: bootstrap $*p < 0.05$ between groups.

FIGURE 8 Effects of CNO injection network communities upon restraint. **(A)** Heatmaps representing the cross-correlations (color scale, Pearson correlation R^2 ; the darker, the stronger) between all structures organized according to (PBS or hM4)-Veh-RS communities (communities have been detected using the allegiance of the (PBS or hM4)-Veh-RS group) for both groups [(PBS or hM4)-Veh-RS and PBS-CNO-RS]. **(B)** Average strength of the communities in (PBS or hM4)-Veh-RS and PBS-CNO-RS group. Statistics: Mann-Whitney non-parametric test; $*p < 0.05$ vs. PBS-CNO for the same community.

FIGURE 9 LHb Inactivation and CNO injection alone present some similarities. **(A)** Heatmap representing the cross-correlations (color scale, Pearson correlation R^2 ; red represent positive, and blue negative, correlations) between all structures sorted by main regions (cortical areas, purple; basal ganglia and septum areas, green; extended amygdala, pink; habenula, red; hippocampus field, yellow; thalamus and hypothalamus area, grey; brainstem area, blue) for PBS-CNO-RS and hM4-CNO-RS. **(B)** Heatmaps of the correlations (R^2 ; the darker the stronger correlation) in PBS-CNO-RS and hM4-CNO-RS groups organized according to PBS-CNO-RS communities (communities extracted on the allegiance matrix of the PBS-CNO-RS group). **(C)** Average strength of the communities in PBS-CNO-RS and hM4-CNO-RS group. Statistics: Mann-Whitney non-parametric test; $*p < 0.05$ indicated between-group difference for the same community.

FIGURE 10 Representation of the structures shared between communities of the different groups. Shared structures (green squares) between (PBS or hM4)-Veh-RS communities and PBS-CNO-RS communities **(A)** and between PBS-CNO-RS communities and hM4-CNO-RS communities **(B)**. Jaccard index in percentage is displayed for each comparison, representing the percentage of corresponding between the two communities indicated (rows and columns).

GRAPHICAL ABSTRACT

GRAPHICAL ABSTRACT TEXT

In this study, using immunohistochemical staining of the immediate early gene *c-fos* and graph theory-based functional correlational analyses, we aimed at unravelling the possible engagement of the lateral habenula (LHb) within the stress response network during acute stress exposure (10-min restraint) in rats. We found that the medial part of the LHb (LHbM) was preferentially engaged, and that this engagement was concomitant to this of structures such as the medial prefrontal cortex (mPFC), the insular cortex (Ins), hypothalamic (PVH) and thalamic (PVT) paraventricular nuclei, the extended amygdala, comprising the Bed nucleus of the stria terminalis (BNST) and the entire amygdala (AMG), as well as the dopaminergic ventral tegmental area (VTA) and the serotonergic dorsal raphe nucleus (RD). This suggests upon stressful situations the LHbM serves as a relay of cortical, thalamic, hypothalamic and temporal information, further transmitted to midbrain monoaminergic systems to probably initiate coping strategies.

CONFLICT OF INTEREST

The authors declare no conflict of interest.

ETHICAL STATEMENT

The authors declare that animals were handled in accordance with ethical requirements enacted by the French authorities and the Strasbourg university who approved the present project (APAFIS #7114).

AUTHOR CONTRIBUTIONS

LL and MM designed the study. LD, LL, MM performed the experiments and analysed the data. AB helped with the restraint procedure. KH, CB, CH helped with the c-fos counting. DB helped with graph theory analyses. VA and YG performed the LC-MS/MS measurements. LL, MM, LD wrote the manuscript.

DATA AVAILABILITY STATEMENT

Data supporting the findings of this study are available upon reasonable request from the corresponding authors.

SUPPORTING INFORMATION

Additional supporting information may be found online in the Supporting Information section at the end of this article.

Figure 1

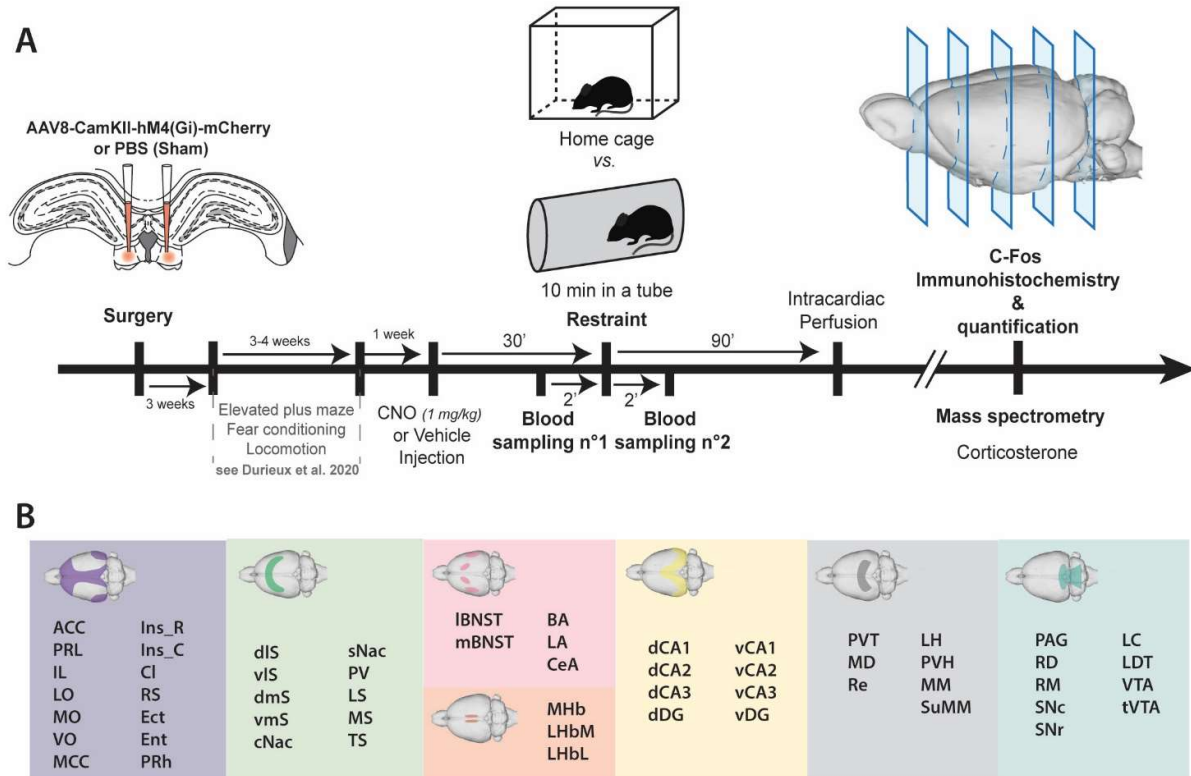


Figure 2

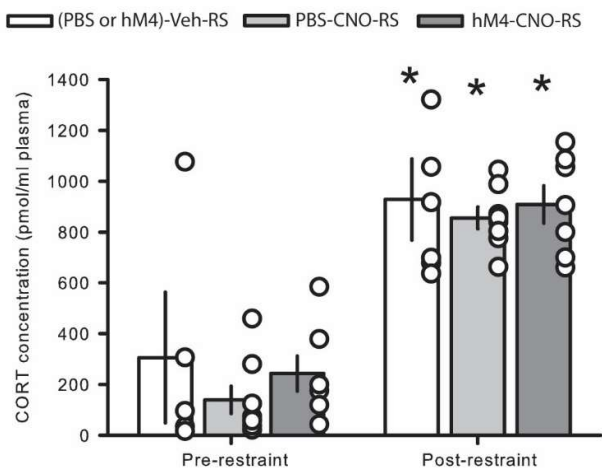


Figure 3

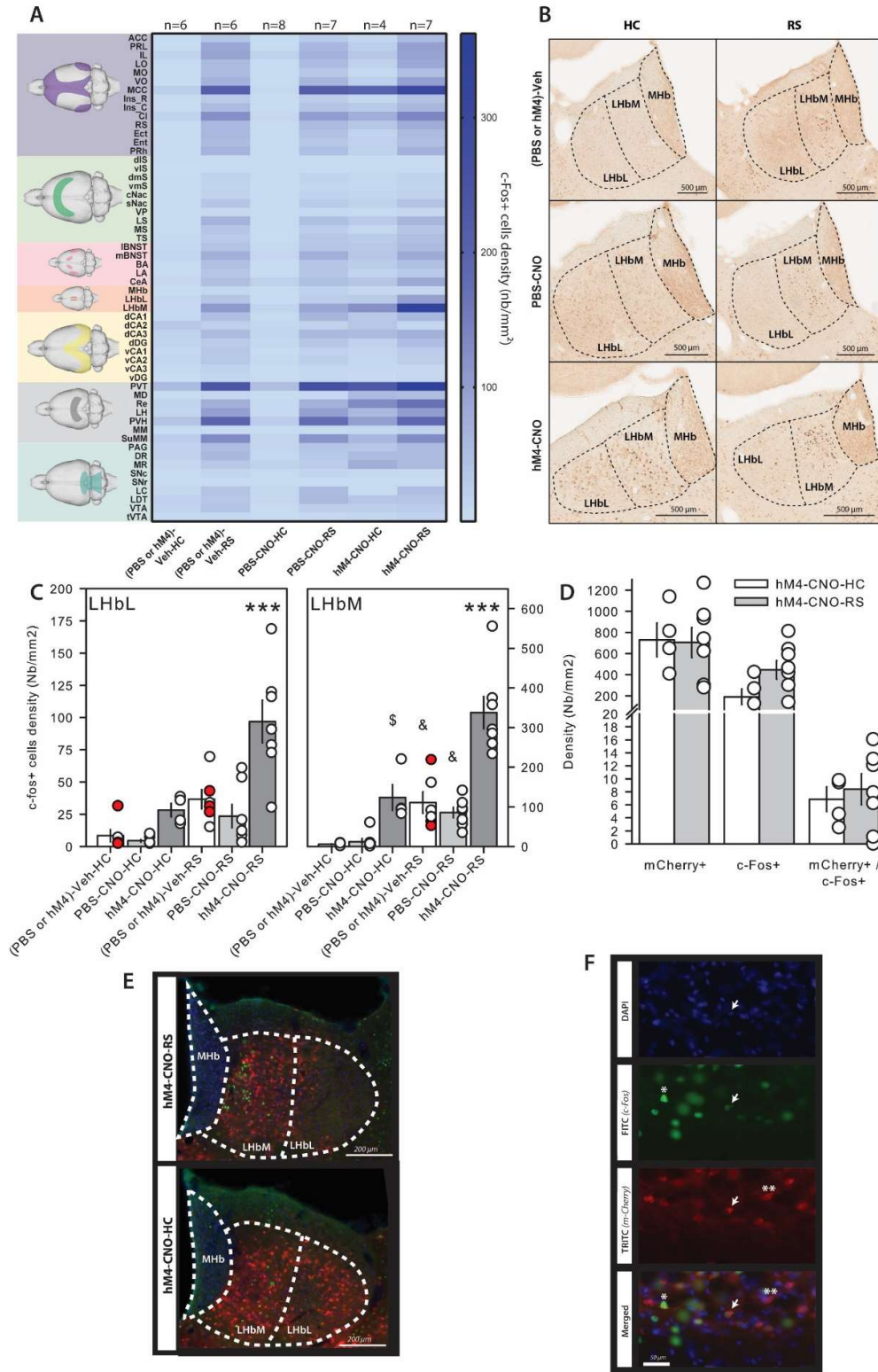
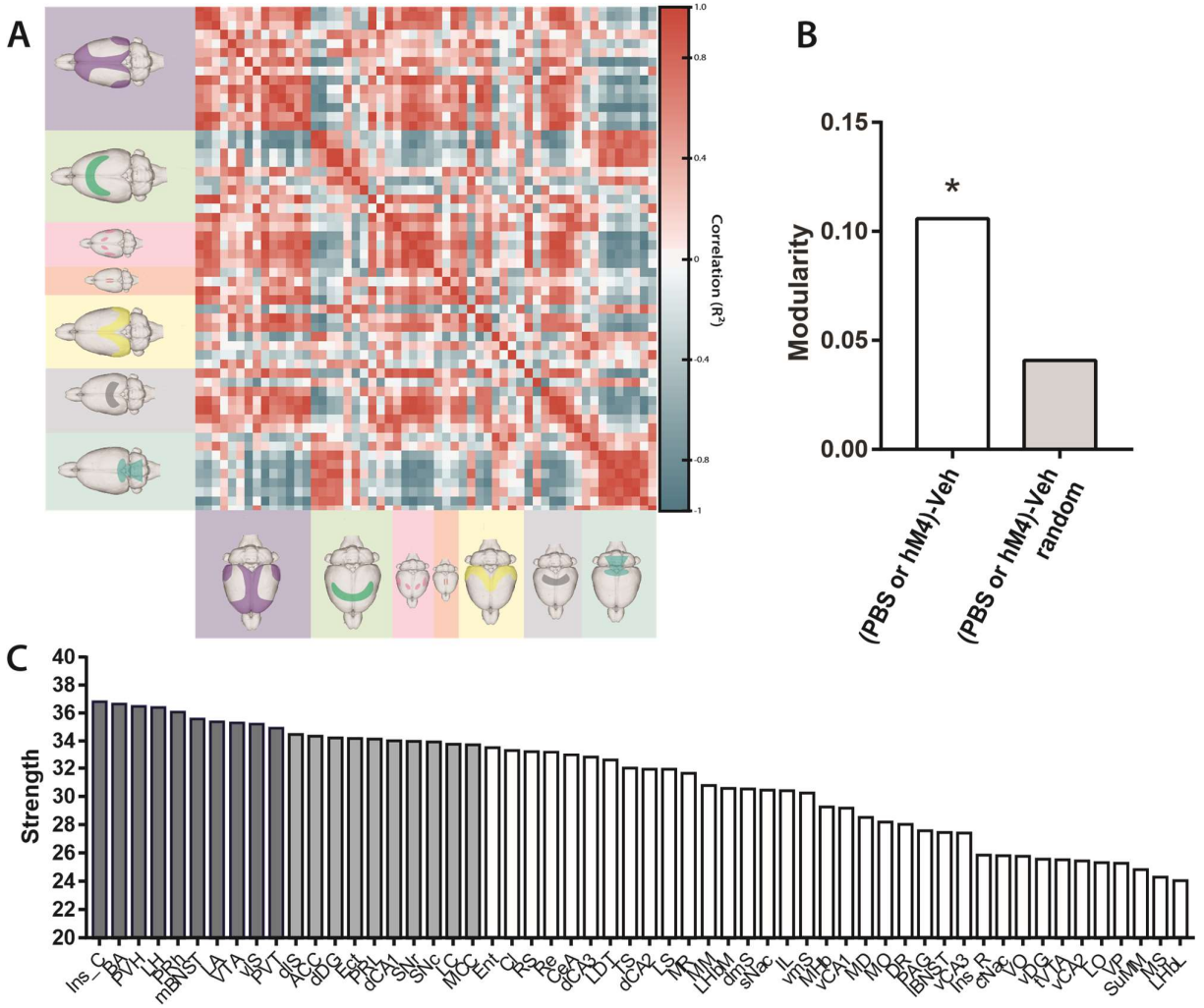


Figure 4



540

Figure 7

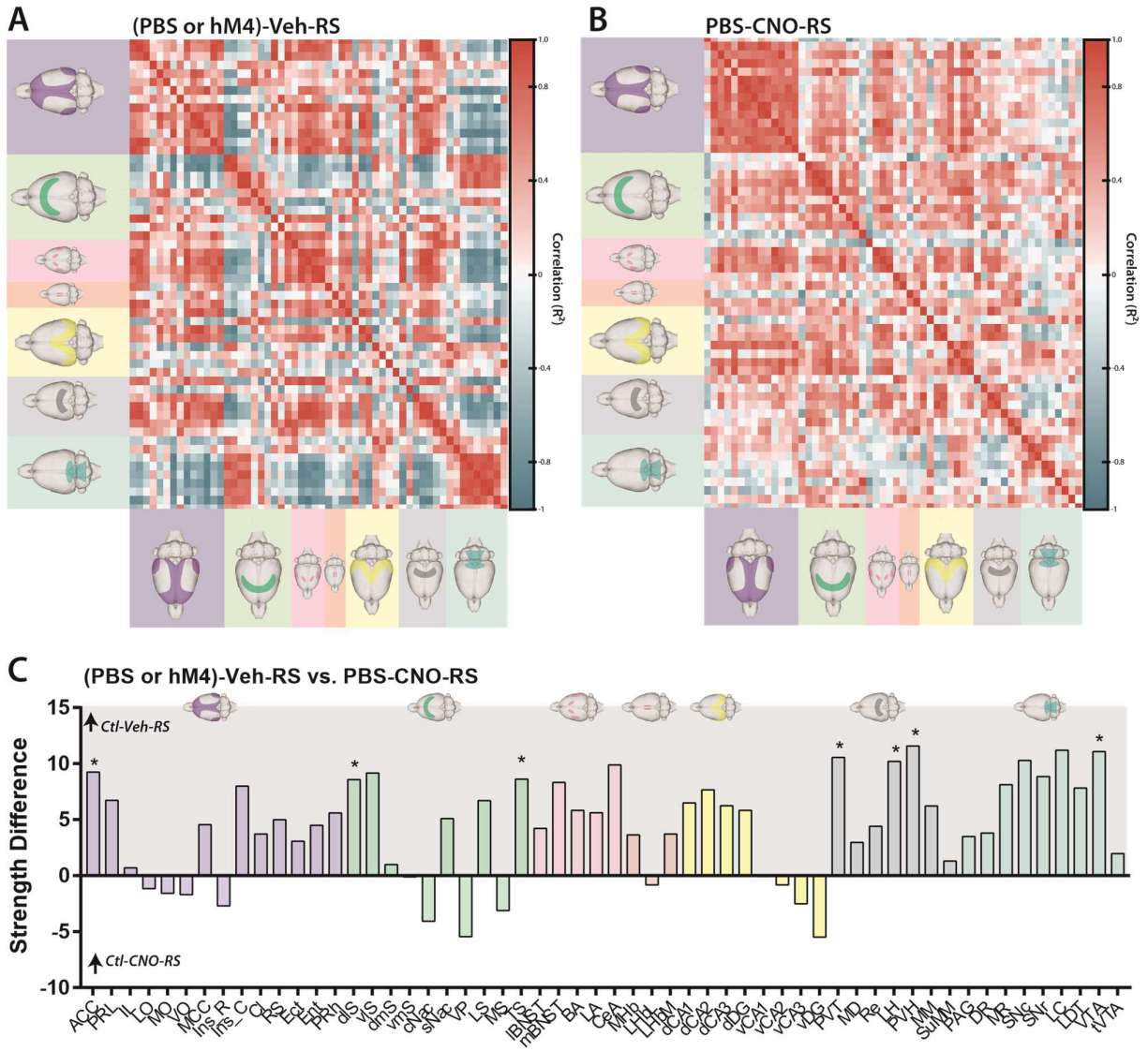
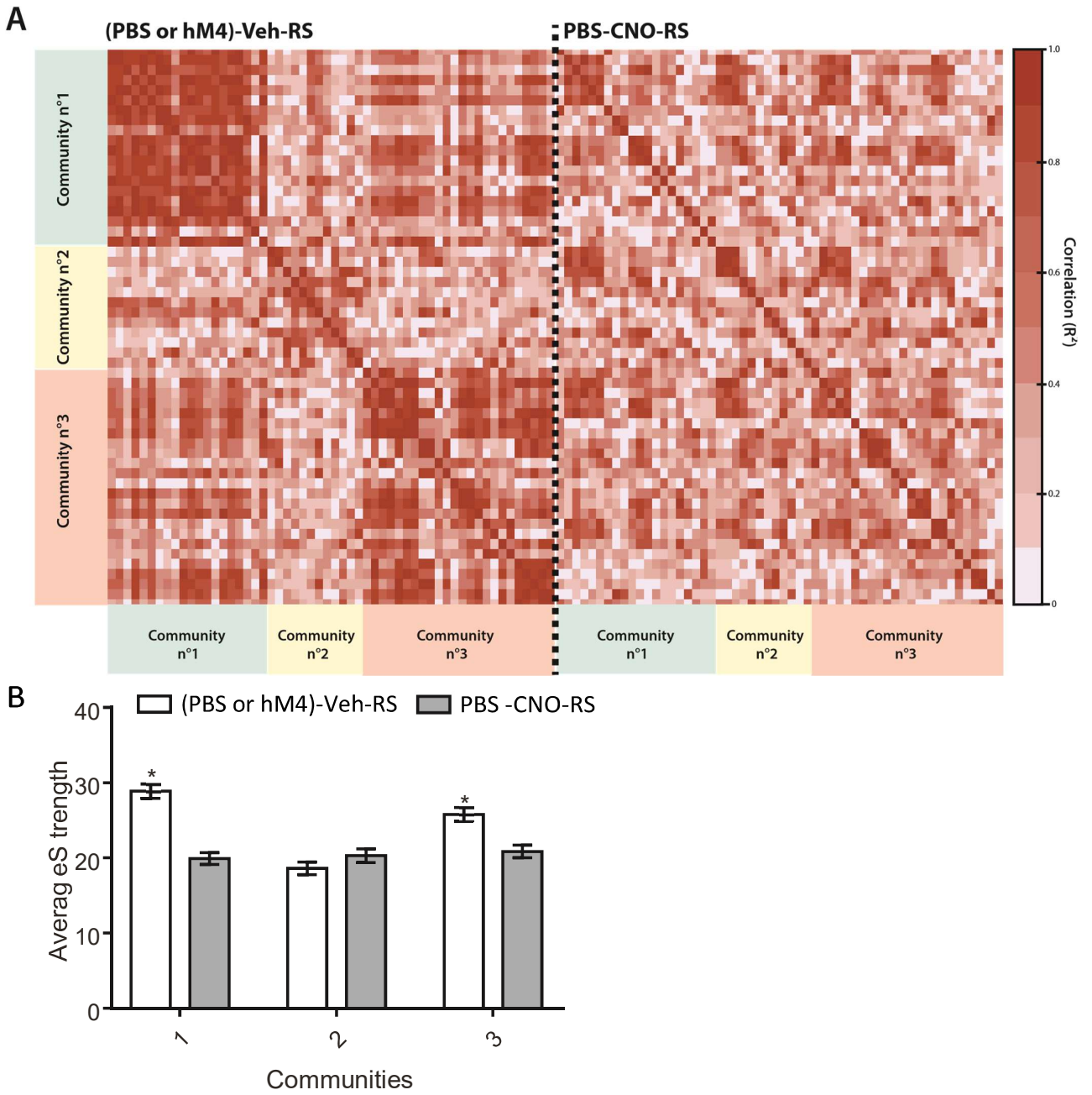


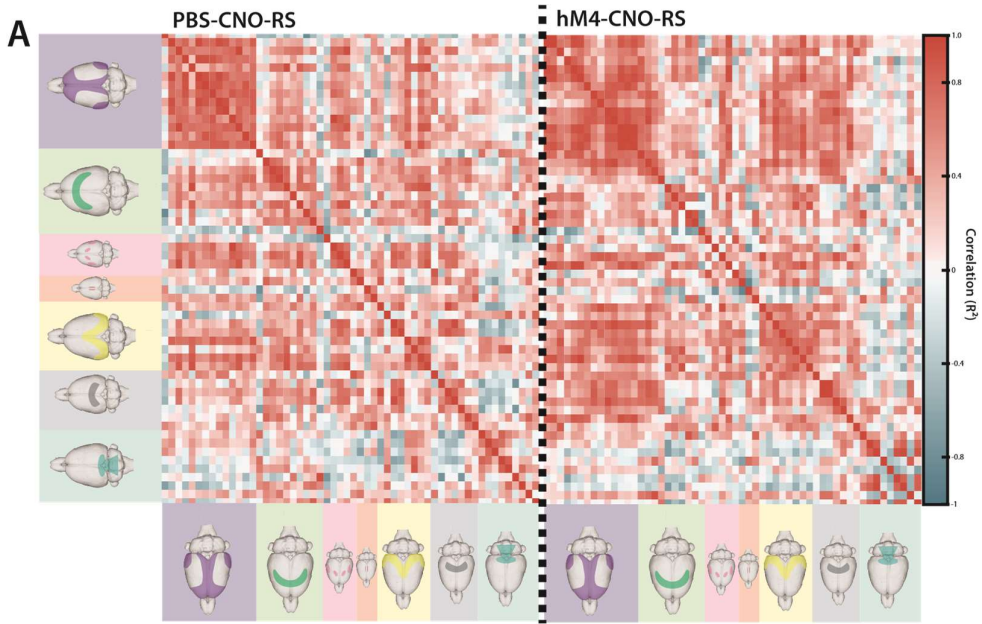
Figure 8

Model: (PBS or hM4)-Veh-RS communities

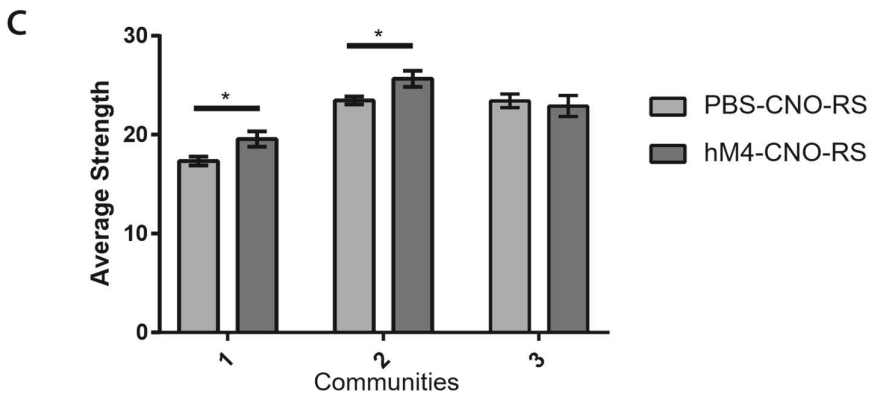
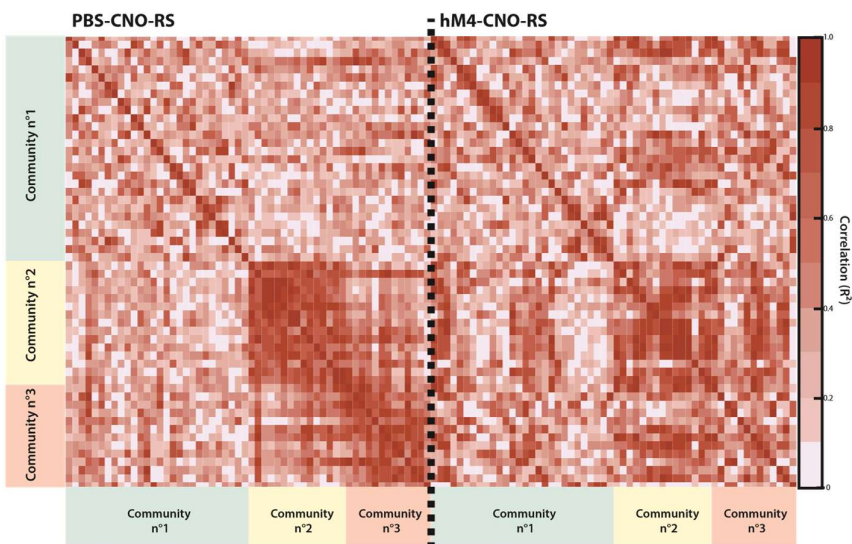


543

Figure 9



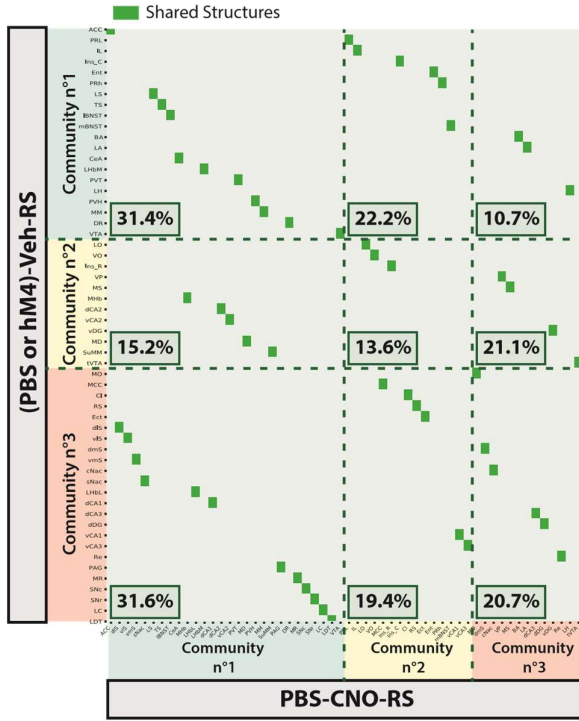
544 **B** Model: PBS-CNO-RS communities



545

Figure 10

546 A



B

